JOPAT Vol 23(1) 1313– 1347, Jan – June. 2024 Edition.

ISSN2636 – 5448 https://dx.doi.org/10.4314/jopat.v23i1.9

Antioxidant, Anti-Inflammatory and Anti-Glycation Activities of Some 4-Aminoantypyrine Derivatives: *In Vitro* and *In Silico* Study

Erazua Ehimen Annastasia[a*], and Babatunde Benjamin Adeleke[a],

[a]*Department of Chemistry, University of Ibadan, Ibadan, Nigeria*

Abstract

Aminoantipyrine exhibits antioxidant and anti-inflammatory effects. However, its potential as an anti-glycating agent has not been extensively studied. This research aims to investigate the antioxidant, anti-inflammatory, and anti-glycation properties of specific derivatives of 4-amino antipyrine through experimental and theoretical methods. Thirteen Schiff bases were synthesized by reacting 4-aminoantipyrine with substituted benzaldehydes, and seven ether derivatives were obtained from these Schiff bases via Williamson ether synthesis. The compounds were characterized using FT-IR, UV-visible, EI-MS, and ^{1}H NMR analyses. Cytotoxicity assessments were conducted using brine shrimp and 3T3 mouse fibroblast cell lines. Molecular descriptors were obtained from Density Functional Theory (DFT) calculations, and molecular docking was used to determine binding affinity. Additionally, in-silico ADMET (adsorption, distribution, metabolism, excretion, and toxicity) screening was performed. The synthesized compounds were evaluated for anti-inflammatory, antioxidant, and anti-glycation properties. The results showed promising activities for three compounds in the anti-inflammatory assay. Five compounds demonstrated significant antioxidant effects, while eight exhibited moderate anti-glycation properties. Compounds S1 and S13 show potential inhibition against the anti-inflammatory, antioxidant, and anti-glycation activities. DFT calculations and molecular docking identified S6, S7, and S9 as the most active compounds. All compounds displayed favorable results in terms of oral bioavailability, lipophilicity, pharmacokinetics, and toxicity prediction. These derivatives of 4-aminoantipyrine were non-toxic and showed potential as drug candidates due to their anti-inflammatory, antioxidant, and anti-glycation properties.

Keywords: 4-Aminoantipyrine; Schiff bases; Anti-inflammatory; Antioxidant; Antiglycation; Oxidative stress; Molecular docking.

Corresponding author's email*: erazuaann@gmail.com*

Introduction

Schiff bases are compounds that contain azomethine groups, and they play a crucial role in synthetic chemistry. They have wide-ranging applications in fields such as biology, medicine, industry, and materials science [1-4]. These compounds are particularly valuable for creating bioactive molecules with desirable properties like anti-inflammatory, analgesic, antioxidant, anticancer, and enzyme immobilization [5-8].

Numerous Schiff bases have been derived from 4-aminoantipyrine [5, 9-11]. Schiff bases derived from 4-aminoantipyrine exhibit scavenging properties against reactive oxygen species (ROS) [12,13]. ROS are generated due to excessive oxygen consumption, leading to oxidative stress and various diseases [14, 15]. Antioxidants play a pivotal role in preventing oxidation and managing oxidative stress, thereby hindering disease progression [16]. It is noteworthy that glycation, oxidative stress, and inflammation are closely interconnected. The exposure to ROS triggers the release of proinflammatory cytokines from cells and is produced during glycation reactions [17]. Elevated glucose levels can result in increased oxidant production, potentially causing chronic oxidative stress and the formation of advanced glycation end products (AGEs) [18]. By managing oxidative stress pathways using antioxidants and glucose regulation, the progression of diabetes-related complications can be impeded [15]. Although the documented anti-inflammatory and antioxidant properties of 4-aminoantipyrine derivatives suggest their potential as antiglycation agents, their role in inhibiting glycation is not extensively discussed in the literature. Therefore, it is necessary to evaluate the potential antiglycation effects of 4-aminoantipyrine. Given the issues of drug tolerance, resistance, and side effects associated with current antioxidant and anti-inflammatory medications, it is crucial to pursue alternative drugs that have minimal or no side effects.

Developing a new drug is a complex and costly process; nevertheless, these challenges can be mitigated through a computational approach. Molecular docking is a widely employed computational method for studying how ligands behave in the binding site of a target protein. It involves predicting the conformation, orientation, and location of the ligand in the active site, as well as calculating binding affinity [19]. Density Functional Theory (DFT), with its various calculation levels, has been effective and reliable in accurately predicting the properties of different compounds. It has played a significant role in determining fundamental compound properties that are not easily achievable through traditional laboratory techniques [20]. Integrating in silico prediction of Absorption, Distribution, Metabolism, Excretion, and Toxicity (ADMET) properties in the early stages of drug discovery is crucial for timely identification of potential pharmacokinetic issues and drug failures [21-23]. This integration facilitates well-informed decision-making in the drug design process before costly and time-consuming clinical trials [24]. ADMET profiling plays a significant role in identifying and optimizing promising drug candidates, enabling the rational design of effective and safe therapeutic agents.

The study focuses on synthesizing Schiff bases and alkyne ethers from 4-aminoantipyrine and different substituted aromatic carbonyl compounds. These compounds were characterized using FT-IR, UV-visible, EI-MS, and 1H NMR techniques. Furthermore, their anti-inflammatory, antioxidant, and antiglycation properties were investigated. Molecular descriptors of the synthesized compounds were determined through DFT optimization. Additionally, the interaction and conformation of the newly formed compounds (ligands) with target proteins were examined through molecular docking. The ADMET properties of the compounds were also assessed to determine their potential for medical applications.

Materials and Methods

All the chemicals and reagents were purchased from commercial sources. Melting points (Mp) were determined using a Buchi M-560 (Japan) instrument in open capillaries. IR spectra (υ, cm^{-1}) were recorded using a Bruker Vector 22 and FTIR-8900 in the range of 4000 to 400 cm^{-1}. The wavelength of maximum absorption was obtained using a Thermo Scientific Evolution 300 UV-Visible spectrophotometer in a chloroform solution. The mass-to-charge ratios (m/e) of the ions produced were determined by EI-MS using a Jeol-600H-1. ^{1}H-NMR spectra were acquired at 400 and 500 MHz using a Bruker Advance spectrometer in DMSO-d6 and MeOD. Chemical shift values are given in parts per million (ppm) for the internal standard, tetramethyl silane (TMS). Acronyms s = singlet, d = doublet, q = quartet, m = multiplet, and t = triplet was used to describe the multiplicity.

Synthesis of Schiff Bases

The Schiff bases (S1-S13) were synthesized according to scheme 1. by the condensation of 4-aminoantipyrine with different aromatic aldehydes [5, 25]. Equimolar amounts of 4-aminoantipyrine and benzaldehyde (5 mmol) were heated in 10 mL of ethanol, in a water bath at 80-85°C for 4-12 hours. Glacial acetic acid was used as the catalyst. TLC was used to monitor the reaction's development. Following the completion of the reaction, the precipitates were filtered, recrystallized, and vacuum dried. The products obtained were elucidated with ^{1}H-NMR, EI-MS, UV-visible, and FT-IR spectroscopy.

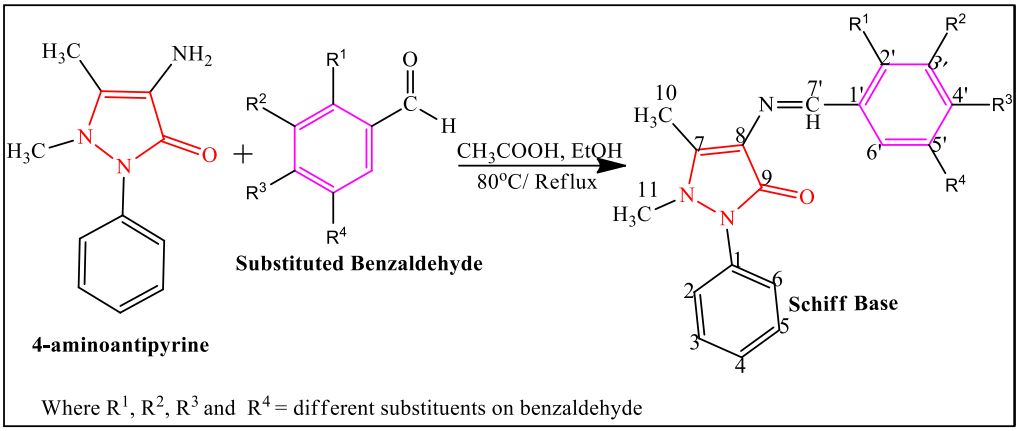

Scheme 1. Synthetic Route for 4-Aminoantipyrine Schiff Bases

Table 1. Description of the substituents on Schiff bases

Compound	R^1	R^2	R^3	R^4
S1	H	**OCH_3**	**OH**	H
S2	**OH**	**OCH_3**	H	H
S3	H	H	**OCH_3**	H
S4	H	H	**CN**	H
S5	H	H	OH	H
S6	**NO_2**	H	H	**OH**
S7	H	**OH**	**OH**	H
S8	**OH**	H	**OH**	H
S9	**OH**	**OH**	H	H
S10	Cl	H	**F**	H
S11	H	**OCH_3**	**CH_3**	H
S12	**OH**	**OH**	**OH**	H
S13	H	**OCH_3**	**OH**	**OCH_3**

Synthesis of Ether-Alkyne Compounds

Ether compounds (E1-E6) with propyne moiety were synthesized from some synthesized 4-aminoantipyrine Schiff bases with OH substituent as reported [26] (Scheme 2). A mixture of anhydrous potassium carbonate (0.5 mmol) and hydroxyl substituted Schiff base (S1, S2, S5, S7, S8, and S13) (0.25 mmol) was stirred at room temperature for 1 hr in DMF (5 ml). To this, propargyl bromide (0.25 mmol) was added and the mixture was stirred for an additional 8-12 hours at room temperature. The development of the reaction was monitored

by a TLC system of n-hexane: ethyl acetate, 6:4. On completion of the reaction, the organic layer of the reaction mixture was extracted using ethyl acetate. Excess ethyl acetate was evaporated off and solid products were obtained as pure compounds.

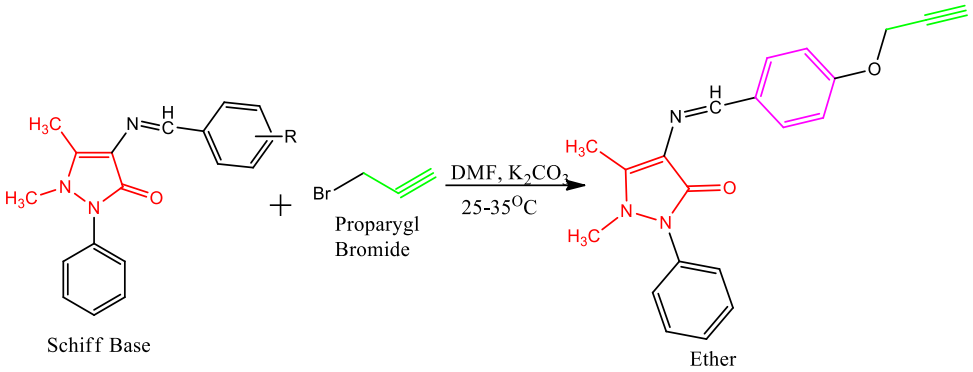

Where R = OH substituent on the Schiff base at different position

Scheme 2: Synthesis of Akyne Ether from Amino-Antipyrine Schiff Bases

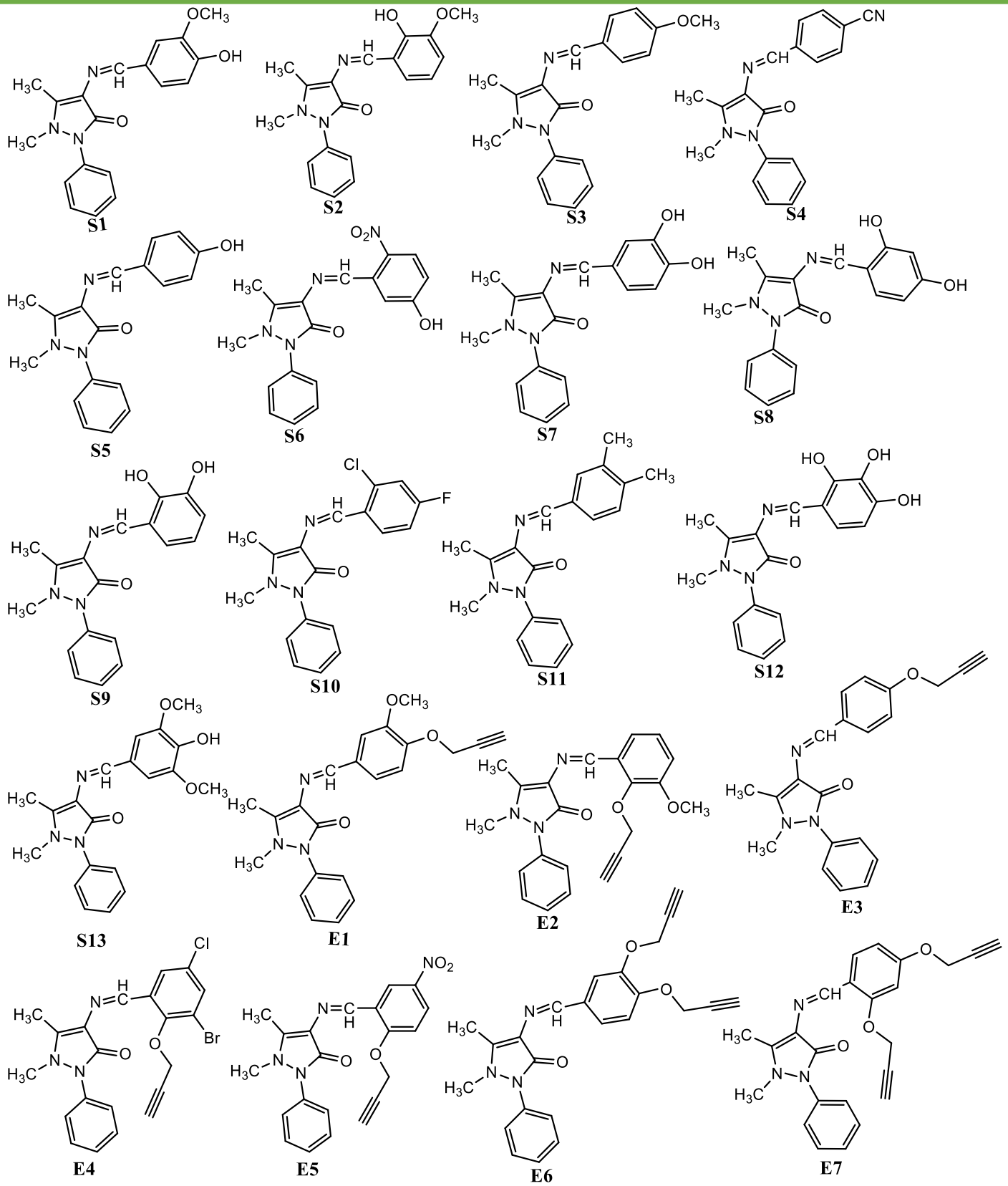

Figure 1: Structure of the Synthesized Compounds

Determination of Cytotoxicity Using Brine Shrimp Lethality Assay

The brine shrimp lethality test, a preliminary screening for cytotoxicity, was conducted using a method described in the literature [27,28]. Brine shrimp eggs were hatched into larvae in a brine solution at 37 ºC. The test sample had 20 mg of compounds in 2 ml of DMSO solvent, creating concentrations of 10, 100 and 1000 µg/ml. After hatching for 48 hours, 10 larvae were added to each vial with 5 ml seawater and incubated at 25-27º C for 24 hours. Etoposide was used as a positive control, with the solvent as a negative control. The Finney computer program analyzed the data to determine mortality rates with 95% confidence.

Determination of Cytotoxicity using MTT Colorimetric Assay

Cytotoxicity was carried out using MTT (3-[4,5-dimethylthiazole-2-yl]-2,5-diphenyl-tetrazoliumbromide) colorimetric test as reported [29]. The Dulbecco's Modified Eagle Medium was used to cultivate the 3T3 (mouse fibroblast) cells. Cells were in 75 cm2 flasks in a 5% CO2 incubator at 37°C and counted during exponential growth. A concentration of 5x104 cells/ml was added to each well of 96-well plates. After overnight incubation, the solvent was replaced with one containing various compound amounts (1 to 30 µM). Two days later, each well received 200 µL of MTT (0.5 mg/ml) and 100 µL of DMSO and incubated for 4 hrs. Absorbance at 540 nm was measured to determine MTT conversion to formazan, calculating cytotoxicity as percent inhibition.

Determination of Anti-Inflammatory Activities using Oxidative Burst Assay

The anti-inflammatory activity was determined using an oxidative burst assay as described by Leah *et al.,* 2020 [30] A chemiluminescence assay was conducted with compound concentrations of 1, 10, and 100 µg/mL, incubated with diluted whole blood in HBSS++ (calcium and magnesium chloride included). Tests were done in white 96-well plates, incubated at 37 ºC for 15 minutes. Post-incubation, luminol and serum opsonized zymosan were added to each well, excluding blank wells with only HBSS++. ROS levels were measured in relative light units, using a luminometer. Ibuprofen was the control.

Determination of Antioxidant Activity using DPPH Radical Scavenging Assay

The antioxidant activity of compounds was analyzed using 2,2-Diphenyl-1-picrylhydrazyl (DPPH) free radical, as described by Sethi *et al.,* 2020 [31]. The DPPH displays a purple color due to its odd electron, which changes to pale yellow when reduced by an antioxidant. This reduction lessens the absorption of the DPPH radical at 515 nm. Test samples were dissolved in 100% DMSO, mixed with DPPH, and incubated at

37° C. The final absorbance was recorded at 515 nm using a microplate reader. The control contained only 100% DMSO, and N-acetyl cysteine and gallic acid were used as standards. The percentage of radical scavenging activity was calculated using a specific equation.

Determination of Antiglycation Activity using Human Serum Albumin Solution

The inhibition of advanced glycation end products was determined by Starowicz and Zielinski (2019). A 200 μL reaction mixture including the test compound (1mM), Human Serum Albumin solution (10 mg/mL), methylglyoxal (14 mM), and a pH 7.4 buffer with sodium azide was prepared. This was incubated in triplicates at 37°C for nine days. Afterward, a varioskan LUX microplate reader was used to check for specific fluorescence. The percentage of inhibition of AGE production was then calculated.

$$\% \text{ Inhibition} = 1 - \frac{\text{Fluorescence of test sample}}{\text{Fluorescence of the control group}} x\ 100 \quad (1)$$

The compounds that exhibited 50% or above percent inhibition were processed for IC_{50} calculations by using various concentrations of test compounds (ranges from 50-1000 µM). To assess the potency of each test compound, it was compared to rutin, the reference inhibitor. (IC_{50} of Rutin = 280.50±1.50µM).

Density Functional Theory Calculations and Molecular Docking

Quantum chemical calculations were done via DFT method using Spartan '14 wavefunction Inc. with the standard 6-31+G* (d) basis set and B3LYP functional (Becke's gradient, exchange correlation [33], and the Lee, Yang, Parr correlation functional [34]. The Global reactivity descriptors that describe the bioactivities of these compounds were calculated based on E_{HOMO} and E_{LUMO} as reported by Koopmans' theorem (35) using the equations 2-5.

Global hardness: $\eta = \frac{E_{LUMO} - E_{HOMO}}{2}$ (2)

Chemical softness $\sigma = \frac{1}{\eta}$ (3)

Electronegativity: $\chi = -\frac{E_{LUMO} + E_{HOMO}}{2}$ (4)

The electrophilicity index [36] $(\omega) = \frac{\mu^2}{2\eta}$ (5)

Molecular docking was done to examine the potential binding mode of the studied compounds with some antioxidant, anti-inflammatory, and antiglycation protein targets to complement the experimental results. The compounds which showed biological activities were utilized as ligands. Cyclooxygenase (COX1 and COX 2), the enzymes that make prostaglandins (PGs) are responsible for the inhibition of Anti-inflammation. Cyclooxygenase-2 (COX-2) (PDB ID: 1OQ5), was selected to investigate the anti-inflammatory activities of the compounds. Glutathione peroxidase (PDB ID: 3KIJ), was selected as the target for antioxidant activities because Glutathione peroxidase-1 is an intracellular antioxidant enzyme that enzymatically reduces hydrogen

peroxide to water to limit its harmful effects. (PDB ID: 4LP5) inhibit was used as an anti-glycation receptor because of the ability of RAGE to inhibit glycation. The 3D Structures of these molecules were obtained from protein databank (www.rcsb.org). The possible binding sites/ active sites of receptors were identified with CASTp and UniProtKB [37]. Proteins were prepared with Chimera 1.14 [38], removing extraneous molecules. Ligands were saved as SDF files and converted to PDBQT format using Autodock 4.2 from PyRX. Grid space was set around the amino acid residues in the active site of the proteins, with grid box parameters recorded in Table 3.1. Autodock Vina from PyRX was used for docking ligands into proteins, obtaining binding affinities [39,40]. UCSF Chimera 1.14 created 3D images of protein-ligand complexes, while Discovery Studio 2020 created 2D molecular interaction representations [41].

The ADME characteristics of the test substances were established using the Swiss ADME web server [42], while toxicity was predicted through ProTox-II [43]. Both servers use a large database to predict essential properties of substances, including physicochemical properties, pharmacokinetics, solubility, and toxicity. Drug-likeness was assessed using rule-based filters [44,45].

Results and Discussion

Twenty compounds, including thirteen Schiff bases and seven alkyne ether, were synthesized with compounds S10, S11, E4, E5, and E6 produced for the first time (Figure 1). All compounds yielded highly. Spectroscopic techniques like FT-IR, UV-visible, EI-MS, and ^{1}HNMR confirmed their chemical structures. Spectroscopic data of the synthesized compounds matched those in the literature [6,26,46]. ^{1}H-NMR spectra were recorded in methanol and DMSO. Imines were identified by frequencies at 1659-1705 cm-1, alkyne ethers by the absence of O-H vibration at 3300-3500 cm-1, and peak at 2100-2124 cm-1 for C≡C. The ^{1}H-NMR spectra showed peaks for aromatic, methyl, and azomethine protons. Acetylenic protons were observed for all alkyne-ether compounds at 3.416-3.702 ppm. EI-MS spectra showed the molecular ion peak M+ and other prominent peaks.

1. 4-((4-hydroxy-3-methoxybenzylidene)amino)-1,5-dimethyl-2-phenyl-1,2-dihydro-3H-pyraz- ol-3-one (S1): Pale yellow crystal; Yield: 82 %; M.p: 207.1-208.3 ^{o}C. ^{1}HNMR (500 MHz, δ ppm MeoD-d_6): 9.395 (s, 1H, $H_{7'}$, N=CH), 7.560 (t, J = 7.5 Hz, 2H, $H_{3,5}$ Ar-H), 7.511 (d, J = 2 Hz, 1H, $H_{2'}$ Ar-H), 7.445 (d, J = 7 Hz, 1H, $H_{6'}$ Ar-H) 7.412 (d, J = 8, 1 Hz, 2H, $H_{2,6}$ Ar-H), 7.221 (dd, J = 8, 1.5 Hz, 1H, H_4 Ar-H), 6.845 (d, J = 8 Hz, 1H, $H_{5'}$ Ar-H), 3.913 (s, 3H, $H_{8'}$, OCH_3) 3.203 (s, 3H, H_{11}, N-CH_3) and 2.475 (s, 3H, H_{10}, CH_3). EI-MS (m/z) 337

[M^++1]. IR ῡ (cm^{-1}): 3653 (O-H), 3105 (C-H Ar), 2942 (CH_3), 1627 (C=O), 1580 (C=N), 1416 (C-O), 1345 (C-N), 1214 (N-N). UV (λ max, $CHCl_3$): 337 nm.

2. 4-((2-hydroxy-3-methoxybenzylidene)amino)-1,5-dimethyl-2-phenyl-1,2-dihydro-3H-pyrazol-3-one (S2):

Yellow crystal; Yield: 89 %; Mp: 233.1-234.4 °C; ^{1}HNMR (400 MHz, δ ppm, DMSO-d_6): 13.011 (s, 1H, $H_{4'}$, OH), 9.673 (s,1H, N=CH, $H_{7'}$), 7.553 (t, *J* = 7.6, 1.6 Hz, 2H, $H_{3,5,}$ Ar-H), 7.409 (dd, *J* = 7.6, 1.2 Hz, 2H, $H_{2,6,}$ Ar-H), 7.375 (d, *J* = 1.2Hz, 1H, $H_{4,}$ Ar-H), 7.059 (dd, *J* = 8, 1.2 Hz, 1H, $H_{6',}$ Ar-H), 7.039 (*J* = 6.8 Hz, 1H, H-$_{4',}$ Ar-H), 6.860 (t, *J* = 8 Hz,1H, $H_{5',}$ Ar-H), 3.796 (s, 1H, $H_{8'}$, OCH_3). 3.202 (s, 3H, H_{11}, N-CH_3) and 2.399 (s, 3H, H_{10}, CH_3. EI-MS (m/z) 337 [M^++1]. FT-IR (Cm^{-1}): 3736 (O-H), 3069 (C-H Ar), 2924 (C-H CH_3), 1664 (C=O), 1593 (C=N), 1487 (C=C), 1419 (C-O bend), 1296 (C-N), 1247 (C-O stretch), 1068 (N-N). UV (λ max, $CHCl_3$): 335 nm.

3. 4-((4-methoxybenzylidene)amino)-1,5-dimethyl-2-phenyl-1,2-dihydro-3H-pyrazol-3-one (S3): Cream crystals; Yield: 78 %; M.p: 171.9-172.5 °C. ^{1}HNMR (500 MHz, δ ppm, MeoD-d_6): 9.455 (s,1H, N=CH, $H_{7'}$), 7.781 (dd, *J* = 8.5, 3 Hz, 2H, $H_{2'6'}$, Ar-H), 7.564 (t, *J* = 8, 1.5 Hz, 2H, $H_{3,5,}$ Ar-H), 7.451 (d, *J* = 7.5,1 Hz, 1H, $H_{4,}$ Ar-H), 7.421 (dd, *J* = 8.5, 1 Hz, 2H, $H_{2,6,}$ Ar-H), 6.991 (d, *J* = 8.5, 1 Hz, 2H, $H_{3',5'}$, Ar-H), 3.838 (s, 3H, $H_{8'}$, OCH_3), 3.215 (s, 3H, H_{11}, N-CH_3) and 2.482 (s, 3H, H_{10}, CH_3). EI-MS (m/z): 321[M^++1]. IR ῡ (cm^{-1}): 3050 (C-H Ar), 2934 (CH_3), 1646 (C=O), 1592 (C=N), 1306 (C-N), 1163 (N-N). UV (λ max, $CHCl_3$): 333 nm.

4.4-(((1,5-dimethyl-3-oxo-2-phenyl-2,3-dihydro-1H-pyrazol-4-yl)imino)methyl) benzonitrile (S4): Yellow powder; Yield: 85 %; M.p: 300-301.4 °C. ^{1}H NMR (500 MHz, δ ppm, DMSO-$d_{6,}$): 9.599 (s,1H, N=CH, $H_{7'}$), 7.980 (d, *J* = 8, 2 Hz, 2H, $H_{2'6'}$, Ar-H), 7.894 (d, *J* = 8.5, 1 Hz, 2H, $H_{3',5'}$, Ar-H), 7.548 (t, *J* = 8, 2 Hz, 2H, $H_{3,5,}$ Ar-H), 7.406 (d, *J* = 7.5 Hz, 1H, $H_{4,}$ Ar-H), 7.373 (dd, *J* = 8.5, 1 Hz, 2H, $H_{2,6,}$ Ar-H), 3.226 (s, 3H, H_{11}, N-CH_3) and 2.475 (s, 3H, H_{10}, CH_3). EI-MS (m/z): 316 [M^++1]. IR ῡ (cm^{-1}): 3062 (C-H Ar), 2925 (CH_3), 2222 (C≡N), 1648 (C=O), 1590 (C=N), 1307 (C-N), 1171 (N-N). UV (λ max, $CHCl_3$): 3360 nm.

5. 4-(4-hydroxybenzylideneamino)-1,2-dihydro-2,3-dimethyl-1-phenylpyrazol-5-one (S5): Cream crystal; Yield: 89 %; M.p: 229.6- 230.1 °C. ^{1}H NMR (500 MHz, δ ppm, DMSO-$d_{6,}$): 9.885 (s, 1H, $H_{4'}$, OH), 9.454 (s,1H, N=CH, $H_{7'}$), 7.642 (d, *J* = 8.5, 2 Hz, 2H, $H_{2'6'}$, Ar-H), 7.524 (t, *J* = 8, 2 Hz, 2H, $H_{3,5,}$ Ar-H), 7.370 (d, *J* = 7.5, 2 Hz, 2H, $H_{2,6,}$ Ar-H), 7.343 (d, *J* = 7.5, 1 Hz, 1H, $H_{4,}$ Ar-H), 6.833 (d, *J* = 8.5, 2 Hz, 2H, $H_{3',5'}$, Ar-H), 3.118 (s, 3H, H_{11}, N-CH_3) and 2.407 (s, 3H, H_{10}, CH_3). EI-MS (m/z): 321[M^++1]. IR ῡ (cm^{-1}): 3591 (O-H), 3060 (C-H Ar), 1605 (C=O), 1578 (C=N), 1389 (C-O bend), 1318 (C-N), 1161 (N-N). UV (λ max, $CHCl_3$): 334 nm.

6. 4-((5-hydroxy-2-nitrobenzylidene)amino)-1,5-dimethyl-2-phenyl-1H-pyrazol-3(2H)-one (S6): Bright orange crystal; Yield: 95 %; M.p: 232.8-234.5 ^{o}C. ^{1}H-NMR (500 MHz, δ ppm, DMSO-$d_{6,}$): 11.098 (s, 1H, $H_{3'}$, OH) 9.510 (s,1H, N=CH, $H_{7'}$), 7.952 (d, *J* = 8.5 Hz, 1H, $H_{5'}$, Ar-H), 7.550 (t, *J* = 8 Hz, 2H, $H_{3,5,}$ Ar-H), 7.504 (d, *J* = 1.5 Hz, 1H, $H_{4,}$ Ar-H), 7.382 (dd, *J* = 6.5, 1 Hz, 2H, $H_{2,6,}$ Ar-H), 7.354 (s, 1H, $H_{6'}$), 3.231 (s, 3H, H_{11}, N-CH_3) and 2.471. EI-MS (m/z): 352 [M^{+}+1]. IR ῡ (cm-1): 3633 (O-H), 3057 (C-H Ar), 2929 (CH_3), 1612 (C=O), 1586 (C=N), 1527 (N=O asymmetric), 1424 (C-O bend), 1292 (C-N), 1354 (N=O symmetric) 1292 (C-N), 1229 (N-N). UV (nm): 248, 288, and 409. UV (λ max, $CHCl_3$): 409 nm.

7. 4-((3,4-dihydroxybenzylidene)amino)-1,5-dimethyl-2-phenyl-1,2-dihydro-3H-pyrazol-3-one (S7): Light brown crystal; Yield: 91 %; M.p: 275.9-276.6 ^{o}C; 1HNMR, (500 MHz, δ ppm, DMSO-d_6): 9.370 (s,1H, $H_{7'}$, N=CH), 9.204 (s, 1H, $H_{3'}$, OH), 7.523 (t, *J* = 8 Hz, 2H, $H_{3,5}$ Ar-H), 7.367 (s, 1H, $H_{2'}$ Ar-H), 7.352 (d, *J* = 7 Hz, 2H, $H_{2,6}$ Ar-H), 7.287 (d, *J* = 2 Hz, 1H, $H_{6'}$ Ar-H), 7.020 (dd, *J* = 8, 2 Hz, 1H, H_4 Ar-H), 6.784 (d, *J* = 8.5 Hz, 1H, $H_{5'}$ Ar-H), 3.451 (q, 1H, $H_{4'}$ OH), 3.114 (s, 3H, H_{11}, N-CH_3) and 2.400 (s, 3H, H_{10}, CH_3). EI-MS (m/z): 323 [M^{+}+1]. IR ῡ (Cm^{-1}): 3495 (O-H), 3062 (C-H Ar), 2943 (C-H CH_3), 1616 (C=O), 1589 (C=N), 1561 (C=C), 1377 (C-O bend), 1289 (C-N), 1266 (C-O stretch), 1071 (N-N); UV (nm): UV (λ max, $CHCl_3$): 338 nm.

8. 4-((2,4-dihydroxybenzylidene)amino)-1,5-dimethyl-2-phenyl-1,2-dihydro-3H-pyrazol-3-one (S8): Yellow crystal; Yield: 90 %; M.p: 229.2-230.0 ^{o}C; ^{1}HNMR, (500 MHz, δ ppm, DMSO-d_6): 13.307 (s, 1H, $H_{2'}$, O-H), 10.045 (s, 1H, $H_{4'}$, O-H), 9.545 (s, 1H, $H_{7',}$ N=CH), 7.538 (t, *J* = 8 Hz, 2H, $H_{3,5}$ Ar-H), 7.381 (dd, *J* = 6.5, 1.5 Hz, 2H, $H_{2,6}$ Ar-H), 7.370 (d, J_4 = 6.5 Hz, 1H, $H_{4,}$ Ar-H), 7.245 (d, *J* = 8.5 Hz, 1H, $H_{6'}$ Ar-H), 6.349 (dd, *J* = 8, 2 Hz, 1H, $H_{5'}$ Ar-H), 6.253 (d, *J* = 2 Hz, 1H, $H_{3'}$ Ar-H), 3.148 (s, 3H, H_{11}, N-CH_3), and 2.349 (s, 3H, H_{10}, CH_3). EI-MS (m/z): 323 [M^{+}+1]. IR ῡ (Cm^{-1}): 3450 (O-H), 3059 (C-H Ar), 2921 (C-H CH_3), 1616 (C=O), 1580 (C=N), 1512 (C=C), 1366 (C-O bend), 1318 (C-N), 1225 (C-O stretch), 1160 (N-N). UV (λ max, $CHCl_3$): 347 nm.

9. 4-((2,3-dihydroxybenzylidene)amino)-1,5-dimethyl-2-phenyl-1,2 -dihydro-3H-pyrazol-3-one (S9): Yellow crystal; Yield: 92 %; M.p: 212.2-214.5 ^{o}C. ^{1}H NMR (400 MHz, δ ppm, DMSO-$d_{6,}$): 13.054 (s, 1H, $H_{2'}$, OH), 9.073 (s, 1H, $H_{3'}$, OH) 9.644 (s, 1H, $H_{7',}$ N=CH), 7.554 (t, *J* = 8 Hz, 2H, $H_{3,5}$ Ar-H), 7.408 (dd, *J* = 8.8 Hz, 2H, $H_{2,6}$ Ar-H), 7.386 (d, J_4 = 8.4 Hz, 1H, $H_{4,}$ Ar-H), 6.900 (d, *J* = 7.6 Hz, 1H, $H_{6'}$ Ar-H), 6.740 (t, *J* = 8 Hz, 1H, $H_{5'}$ Ar-H), 6.586 (dd, *J* = 8, 1.2 Hz, 1H, $H_{4'}$ Ar-H), 3.159 (s, 3H, H_{11}, N-CH_3), and 2.402 (s, 3H, H_{10}, CH_3). EI-MS (m/z): 323 [M^{+}+1]. IR ῡ (cm-1): 3453 (O-H), 2943 (CH_3), 1659

(C=O), 1563 (C=N), 1367 (C-O bend), 1267 (C-N), 1200 (N-N). UV (λ max, $CHCl_3$): 335 nm.

10. 4-((2-chloro-4-fluorobenzylidene)amino)-1,5-dimethyl-2-phenyl-1,2-dihydro-3H-pyrazol -3-one (S10): Yellow crystal; Yield: 94 %; M.p: 210.0-211.3 °C. ^{1}H NMR (400 MHz, δ ppm DMSO-d_6): 9.909 (s, 1H, $H_{7'}$, N=CH), 8.216 (dd, J = 8.8 Hz, 1H, $H_{6'}$ Ar-H), 7.546 (d, *J* = 8 Hz, 2H, $H_{3,5}$ Ar-H), 7.494 (d, *J* = 2.4 Hz, 1H, H_4, Ar-H), 7.400 (d, *J* = 8.4 Hz, 2H, $H_{2,6}$ Ar-H), 7.358 (s, IH, $H_{3'}$ Ar-H) 7.341 (dd, J = 8.4 Hz, 1H, $H_{5'}$ Ar-H), 3.212 (s, 3H, H_{11}, N-CH_3), and 2.466 (s, 3H, H_{10}, CH_3). EI-MS (m/z): 343 [M^++1]. IR ῡ (cm-1): 3069 (C-H Ar), 2920 (CH_3), 1651 (C=O), 1593 (C=N), 1306 (C-N), 1163 (N-N). UV (λ max, $CHCl_3$): 338 nm.

11. 4-((3,4-dimethylbenzylidene)amino)-1,5-dimethyl-2-phenyl-1,2-dihydro-3H-pyrazol-3-one (S11): Pale yellow crystal; Yield: 89 %; M.p: 179.6-180 ° C. ^{1}H NMR (400 MHz, δ ppm MeOD-d_6,): 9.455 (s, 1H, $H_{7'}$, N=CH), 7.592 (s, IH, $H_{2'}$ Ar-H), 7.569 (d, *J* = 7.6 Hz, 1H, H_4, Ar-H),7.550 (d, *J* = 7.6 Hz, 2H, $H_{3,5}$ Ar-H), 7.456 (d, J = 7.6 Hz, 1H, $H_{6'}$ Ar-H), 7.414 (d, *J* = 8.8, 1.2 Hz, 2H, $H_{2,6}$ Ar-H), 7.358 (s, IH, $H_{3'}$ Ar-H) 7.192 (dd, J = 7.6 Hz, 1H, $H_{5'}$ Ar-H), 3.223 (s, 3H, H_{11}, N-CH_3), 2.491 (s, 3H, H_{10}, CH_3), and 2.296 (s, 6H, $H_{2',3'}$, CH_3). EI-MS (m/z) 319 [M^++1]. IR ῡ (cm-1): 3051 (C-H Ar), 2922 (CH_3), 1650 (C=O), 1587 (C=N), 1300 (C-N), 1136 (N-N). UV (λ max, $CHCl_3$): 331 nm.

12. 4-((2,3,4-trihydroxybenzylidene)amino)-1,5-dimethyl-2-phenyl-1,2-dihydro-3H-pyrazol-3-one (S12): Dark yellow crystal; Yield: 90 %; M.p: 257.5-261.2 °C. ^{1}HNMR (500 MHz δ, ppm, DMSO-d6): 13.411 (s, 1H, OH, H-2'), 9.519 (s, 1H, OH, H-4'), 9.519 (s, 1H, $H_{7'}$, N=CH), 8.396 (s, 1H, H-3', OH), 7.540 (t, *J* = 7.5 Hz, 2H, $H_{3,5}$ Ar-H), 7.384 (dd, *J* = 7.2 Hz, 2H, $H_{2,6}$, Ar-H), 7.363 (d, *J* = 2 Hz, 1H, H_4, Ar-H), 6.753 (d, J = 8.5 Hz, 1H, $H_{6'}$ Ar-H), 6.375 (dd, J = 8 Hz, 1H, $H_{5'}$ Ar-H), 3.156 (s, 3H, H_{11}, N-CH_3), and 2.491 (s, 3H, H_{10}, CH_3). EI-MS (m/z): 339[M^++1]. IR ῡ (cm-1): 3438 (O-H), 2926 (CH_3), 1610 (C=O), 1508 (C=N), 1393 (C-O bend), 1319 (C-N), 1207 (N-N). UV (λ max, $CHCl_3$): 245 nm.

13. 4-(4-hydroxy-3,5-dimethoxybenzylidene)amino)-1,5-dimethyl-2-phenyl-1,2-dihydro-3H-pyrazol-3-one (S13): Off white powder; Yield: 95 %; M.p: 255.5-257.0 °C. ^{1}H-NMR (400 MHz, *δ* ppm, DMSO-d_6): 9.446 (s, 1H, $H_{7'}$, N=CH), 8.846 (S, 1H, $H_{5'}$,OH), 7.535 (t, *J* = 7.6 Hz, 2H, $H_{3,5}$ Ar-H), 7.379 (dd, *J* = 7.2 Hz, 2H, $H_{2,6}$, Ar-H), 7.360 (d, *J* = 7.2 Hz, 1H, H_4, Ar-H), 7.088 (s, 2H, $H_{2'6'}$ Ar-H), 3.816 (s, 6H, $H_{8'9'}$, OCH_3) 3.029 (s, 3H, H_{11}, N-CH_3), and 2.435 (s, 3H, H_{10}, CH_3). EI-MS (m/z): 367 [M^++1]. IR ῡ (cm-1): 3567 (O-H), 3158 (C-H Ar), 2968 (CH_3), 1634

(C=O), 1588 (C=N), 1332 (C-N), 1210 (N-N). UV (λ max, $CHCl_3$): 341 nm.

14. 4-((3-methoxy-4-(prop-2-yn-1-yloxy)benzylidene)amino)-1,5-dimethyl-2-phenyl-1,2-dihydro -3H-pyrazol-3-one (E1): Brown solid; Yield: 91 %; M.p: 141.9-142.8 ºC. ^{1}H NMR spectrum (500 MHz, δ ppm, DMSO-d_6): 9.490 (s, 1H, $H_{7'}$, N=CH), 7.535 (t, J = 8.5 Hz, 2H, $H_{3,5}$ Ar-H), 7.479 (d, J = 1.5 Hz, 1H, $H_{2'}$, Ar-H), 7.372 (d, J = 7.2 Hz, 1H, H_4, Ar-H), 7.357 (dd, J = 8.5 Hz, 2H, $H_{2,6}$, Ar-H), 7.287 (dd, J= 8, 2 Hz, 1H, $H_{6'}$, Ar-H), 7.091 (dd, J = 8.4 Hz, 1H, $H_{5'}$, Ar-H), 4.839 (d, J = 2.5 Hz, 2H, $H_{1''}$, CH_2), 3.593 (t, J = 2.5 Hz, 1H, $H_{3''}$, C≡C-H), 3.830 (s, 3H, H-8', OCH_3), 3.145 (s, 3H, H_{11}, N-CH_3), and 2.442 (s, 3H, H_{10}, CH_3). EI-MS (m/z): 375 [M^++1]. IR ῡ (cm^{-1}): 3287(-C≡C-H), 3079 (C-H Ar), 2865 (=C-H), 2129 (C≡C), 1652 (C=O), 1599 (C=N). UV (λ max, $CHCl_3$): 338 nm.

15. 4-((3-methoxy-2-(prop-2-yn-1-yloxy)benzylidene)amino)-1,5-dimethyl-2-phenyl-1,2-dihydro-3H-pyrazol-3-one (E2): Cream solid; Yield: 93 %; M.p: 215.1-216.4 ºC. ^{1}H NMR (500 MHz, δ ppm, DMSO-d_6): 9.856 (s, 1H, $H_{7'}$, N=CH), 7.639 (d, J = 7.5, 1.5Hz, 1H, $H_{6'}$, Ar-H), 7.532 (t, J = 8.5, 2 Hz, 2H, $H_{3,5}$ Ar-H), 7.372 (d, J = 7.5 Hz, 1H, H_4, Ar-H), 7.363 (dd, J = 8.5 Hz, 2H, $H_{2,6}$, Ar-H),7.163 (t, J = 8 Hz, 1H, $H_{5'}$, Ar-H), 7.115 (dd, J = 8, 1.5 Hz, 1H, $H_{4'}$, Ar-H), 4.739 (d, J = 2.5 Hz, 2H, $H_{1''}$, CH_2), 3.418 (t, J = 2.5 Hz, 1H, $H_{3''}$, C≡C-H), 3.828 (s, 3H, H-8', OCH_3), 3.169 (s, 3H, H_{11}, N-CH_3), and 2.439 (s, 3H, H_{10}, CH_3). EI-MS: m/z:336 [M^++1]. IR ῡ (cm-1): 3284(-C≡C-H), 3074 (C-H Ar), 2835 (=C-H), 2119 (C≡C), 1651 (C=O), 1572 (C=N), 1300(C-N). UV (nm): 333.

16. 1,5-dimethyl-2-phenyl-4-((4-(prop-2-yn-1-yloxy)benzylidene)amino-1,2-dihydro-3H-pyrazol-3-one (E3): Pale yellow solid, Yield: 68 %; M.p: 155.9-157.0 ºC ^{1}H (500MHz, δ ppm DMSO-d_6): 9.513 (s, 1H, $H_{7'}$, N=CH), 7.770 (d, J = 9, 2 Hz, 2H, $H_{2'6'}$, Ar-H), 7.531 (t, J = 8, 2 Hz, 2H, $H_{3,5}$ Ar-H), 7.374 (d, J = 8.5 Hz, 1H, H_4, Ar-H), 7.357 (dd, J = 8.5 Hz, 2H, $H_{2,6}$, Ar-H), 7.063 (dd, J = 9, 2 Hz, 2H, $H_{3',5'}$, Ar-H), 4.854 (d, J = 2.5 Hz, 2H, $H_{1''}$, CH_2), 3.595 (t, J = 2.5 Hz, 1H, $H_{3''}$, C≡C-H), 3.143 (s, 3H, H_{11}, N-CH_3), and 2.429 (s, 3H, H_{10}, CH_3). EI-MS (m/z): 345 [M^++1]. IR ῡ (cm-1): 3265 (-C≡C-H), 3053 (C-H Ar), 2984 (CH_3), 2926 (=C-H), 2110 (C≡C), 1641 (C=O), 1572 (C=N), 1377 (C-N). UV (λ max, $CHCl_3$): 334 nm.

17. 4-((3-bromo-5-chloro-2-(prop-2-yn-1-yloxy)benzylidene) amino)-1,5-dimethyl-2-phenyl-1,2-dihydro-3H-pyrazol-3-one (E4): Yellow solid, 77 %; M.p: 148.5-1449.9 ºC. ^{1}H NMR spectrum (500 MHz, δ ppm DMSO-d_6): 9.77 (s, 1H, $H_{7'}$, N=CH), 8.015 (d, J = 2.5 Hz, 1H, $H_{6'}$, Ar-H), 7.833 (d, J = 2.5 Hz, 1H, $H_{4'}$, Ar-H), 7.546 (t, J = 8 Hz, 2H, $H_{3,5}$ Ar-H), 7.403 (dd, J = 7.5 Hz, 2H, $H_{2,6}$, Ar-H), 7.379 (d, J = 8 Hz, 1H, H_4, Ar-H), 4.755 (d, J = 2.5 Hz, 2H, $H_{1''}$, CH_2), 3.582 (t, J = 2.5

Hz, 1H, $H_{3''}$, C≡C-H), 3.224 (s, 3H, H_{11}, N-CH_3), and 2.476 (s, 3H, H_{10}, CH_3). EI-MS (m/z): 336 [M^++1]. IR ῡ (cm-1): 3293 (C≡C-H), 3210 (C-H Ar), 3063 (CH_3), 2926 (=C-H), 2124 (C≡C), 1660 (C=O), 1586 (C=N), 1301 (C-N). UV (λ max, $CHCl_3$): 349 nm.

18. 1,5-dimethyl-4-((2-nitro-5-(prop-2-yn-1-yloxy)benzylidene)amino-2-phenyl-1,2-dihydro-3H-pyrazol-3-one (E5): Yellow solid, 91 %; M.p: 150.8 -152.3 ^oC. ^1H NMR spectrum (500 MHz, δ ppm, DMSO-d_6): 9.926 (s, 1H, $H_{7'}$, N=CH), 8.069 (d, *J* = 9 Hz, 1H, $H_{3'}$, Ar-H), 7.756 (d, *J* = 2.5 Hz, 1H, $H_{6'}$, Ar-H), 7.550 (t, *J* = 8 Hz, 2H, $H_{3,5}$, Ar-H), 7.411 (d, *J* = 7.5 Hz, 1H, H_4, Ar-H), 7.375 (dd, *J* = 7.5 Hz, 2H, $H_{2,6}$, Ar-H), 7.210 (d, *J* = 9 Hz, 1H, $H_{4'}$, Ar-H), 5.015 (d, *J* = 2.5 Hz, 2H, $H_{1''}$, CH_2), 3.702 (t, *J* = 2.5 Hz, 1H, $H_{3''}$, C≡C-H), 3.240 (s, 3H, H_{11}, N-CH_3), and 2.477 (s, 3H, H_{10}, CH_3). EI-MS (m/z): [M^++1]. IR ῡ (cm-1): 3289 (-C≡C-H), 3252 (C-H Ar), 3061 (CH_3), 2924 (=C-H), 2123 (C≡C), 1655 (C=O), 1575 (C=N), 1337 (C-N). UV (λ max, $CHCl_3$): 290 nm.

19. 4-((3,4-bis(prop-2-yn-1-yloxy)benzylidene)amino)-1,5-dimethyl-2-phenyl-1,2-dihydro-3H-pyrazol-3-one (E6): Yellow solid, 75 %; M.p: 169.5-170.0 ^oC. ^1H NMR spectrum (500 MHz, δ ppm, DMSO-d_6): 9.766 (s, 1H, $H_{7'}$, N=CH), 7.871 (d, *J* = 8 Hz, 1H, $H_{6'}$, Ar-H), 7.553 (t, *J* = 8 Hz, 2H, $H_{3,5}$, Ar-H), 7.473 (dd, *J* = 8.5 Hz, 2H, $H_{2,6}$, Ar-H), 7.356 (d, *J* = 7 Hz, 1H, H_4, Ar-H), 7.116 (d, *J* = 2.5 Hz, 1H, $H_{2'}$, Ar-H), 6.924 (d, *J* = 8 Hz, 1H, $H_{5'}$, Ar-H), 4.980 (d, *J* = 2.5 Hz, 2H, $H_{1''}$, CH_2), 4.862 (d, $J_{1''',3'''}$ = 2.5 Hz, 1H, H-1''') 3.590 (t, *J* = 2.5 Hz, 1H, $H_{3''}$, C≡C-H), 3.579 (t, $J_{3''',1'''}$ = 2.5 Hz, 1H, H-3'''), 3.214 (s, 3H, H_{11}, N-CH_3), and 2.432 (s, 3H, H_{10}, CH_3). EI-MS (m/z): 399 [M^++1]. IR ῡ (cm-1): 3297 (-C≡C-H), 3267 (C-H Ar), 3044 (CH_3), 2925 (=C-H), 2117 (C≡C), 1631 (C=O), 1598 (C=N), 1338 (C-N). UV (λ max, $CHCl_3$): 337 nm.

20. 4-((2,4-bis(prop-2-yn-1-yloxy)benzylidene)amino)-1,5-dimethyl-2-phenyl-1,2-dihydro-3H-pyrazol-3-one (E7): Yellow solid, 93 %; M.p: 185.9-187.3 ^oC. ^1H NMR spectrum (500 MHz, δ ppm, DMSO-d_6): 9.467 (s, 1H, $H_{7'}$, N=CH), 7.983 (d, *J* = 8.5 Hz, 1H, $H_{6'}$, Ar-H), 7.527 (t, *J* = 8 Hz, 2H, $H_{3,5}$, Ar-H), 7.373 (dd, *J* = 7.5 Hz, 2H, $H_{2,6}$, Ar-H), 7.348 (d, *J* = 7 Hz, 1H, H_4, Ar-H), 6.756 (d, *J* = 2 Hz, 1H, $H_{3'}$, Ar-H), 6.725 (d, *J* = 9 Hz, 1H, $H_{5'}$, Ar-H), 4.890 (d, *J* = 2.5 Hz, 2H, $H_{1''}$, CH_2), 4.853 (d, $J_{1''',3'''}$ = 2.5 Hz, 1H, H-1''') 3.598 (t, *J* = 2.5 Hz, 1H, $H_{3''}$, C≡C-H), 3.581(t, $J_{3''',1'''}$ = 2.5 Hz, 1H, H-3'''), 3.134 (s, 3H, H_{11}, N-CH_3), and 2.422 (s, 3H, H_{10}, CH_3). EI-MS (m/z): 399 [M^++1]. IR ῡ (cm-1): 3226 (-C≡C-H), 3088 (C-H Ar), 3011 (CH_3), 2934 (=C-H), 2117 (C≡C), 1640 (C=O), 1575 (C=N), 1377 (C-N). UV (λ max, $CHCl_3$): 337 nm.

Cytotoxicity

The percentage mortality obtained from the Brine Shrimp Lethality Assay showed that the

synthesized compounds were not cytotoxic. Similarly, the percentage inhibition obtained from MTT colorimetric assay against mouse fibroblast cells indicates that the synthesized compounds were non-cytotoxic against normal cell lines.

Anti-inflammatory, Antioxidant, and Antiglycation Activities

Compounds S9, S12, and S1 have excellent anti-inflammatory activities, and compound S9 with hydroxyl substituents on ortho and meta positions performed better than the standard drug (Table 2). S7 and S8 with the same substituent as S9 showed poor activity. S1 with hydroxyl and methoxy substituents had excellent activity while S2 despite similar substituents as S1, had low activity. S12 with trihydroxy substituents also possesses anti-inflammatory activity. It was observed that all compounds with significant activity possess OH or OCH_3. This study showed that the type and position of substituents is a determining factor for compound bioactivity**.**

Compound S1 demonstrated high antioxidant activity (IC50 = 111.10±1.80), while S9 and S12 also had significant activities (IC50 = 29.10±1.08 and 40.90±1.30). S7 and S13 showed moderate activity (IC50 = 214.80±3.58 and 297.20±1.00), but others had none (Table 2). Despite similar structures with some bioactive compounds in the series, S8 and S3 lacked activity, implying that activity depends not just on the substituent type but also on its position, as reported by Teran *et al* [47].

Five Schiff bases and three alkyne compounds demonstrated antiglycation activity. S6 showed very good activity (IC_{50} = 321.16±1.70 µM) which was very close to that of the standard rutin (IC_{50} = 280.50±1.50 µM). E4 and S1 also showed good activity (IC50 = 526.65±2.66 and IC50 = 575.3±1.80 µM). E7, S6, E4, S13, and S5 had moderate activity, with S5 being least active. Other compounds were inactive (Table 2). It is worthy of note that compounds S1 and S13 with OH and OCH_3 substituents possess antioxidant, anti-inflammatory, and antiglycation activities (Table 2).

Table.2: Antioxidant, Anti-inflammatory, and Antiglycation Activities

Sample code	Antioxidant (IC_{50} ± SEM (µM)	Anti-inflammation (IC_{50} ± SEM (µM)	Antiglycation (IC_{50} ± SEM (µM)
S1	111.10±1.80	1.80±0.14	575.30±01.80
S2	-	-	-
S3	-	-	-
S4	-	-	-

S5	-	-	856.80±01.80
S6	-	-	321.16±1.70
S7	214.80±3.58	-	638.8±02.70
S8	-	-	-
S9	29.10±1.08	0.01±0.02	
S10	-	-	-
S11	-	-	-
S12	40.90±1.30	1.50±0.03	-
S13	297.20±1.00	13.40±0.12	842.51±2.40
E1	-	-	-
E2	-	-	-
E3	-	-	-
E4	-	-	721.32±3.29
E5	-	-	526.65±2.66
E6	-	-	-
E7	-	-	628.6±2.80
N-acetyl-L-Cystine	111.60±2.40	-	-
Gallic Acid	22.80±1.35	-	-
Ibuprofen	-	11.20±1.90	-
Rutin	-	-	282.40±0.80

- = Not calculated (because of % inhibition shown was less than 50% at100 µg/mL.

Calculated Descriptors of the Bioactive Compounds

DFT studies were used to generate molecular descriptors for bioactive compounds. The HOMO and LUMO energies, known as frontier molecular orbitals, illustrate a molecule's electronic properties, reactivity, and stability. Higher HOMO and lower LUMO values indicate better interaction ability [48,49], as seen in compounds S13 and S1. The energy difference between the HOMO and LUMO orbital known as band gap (BG), gives information on the reactivity and stability of a molecule, large BG signifies stability, while small BG indicates reactivity [50,51]. S5 with the highest BG showed least antiglycation activities and no anti-inflammatory and antioxidant potential. While compounds S6 and S9 with least BG show good inhibitory potential. This trend is the same for the experimental results.

Chemical potential (µ) is a measure of the ability of a molecule to cause a chemical reaction due to internal chemical energy or

external energy [51]. A lower value of μ leads to lower binding energy and better interaction [52]. A good correlation was observed between these values and the binding energy of the compounds. It was observed that S12, S9, S6, and S1 with lower values of μ had significant bioactivity than compounds S5, S13 and E7 with higher values of μ.

Table 2: Selected Molecular Descriptors for the Bioactive Compounds

η: global hardness; σ: global softness; μ: chemical potential; ω: global electrophilicity index; χ: electronegativity, PSA: polar surface area and POL: polarizability.

Code	E_{HOMO} (eV)	E_{LUMO} (eV)	BG (eV)	η	σ	μ	ω (eV)	χ	DM (Debye)	PSA	POL
S1	-5.70	-2.22	3.48	1.74	0.58	-3.96	4.51	3.96	8.94	56.46	72.32
S5	-5.24	-1.18	4.06	2.03	0.49	-3.21	2.54	3.21	4.63	42.63	66.46
S6	-5.23	-2.70	2.53	1.26	0.79	-3.97	6.21	3.97	9.06	76.02	68.32
S7	-5.22	-1.18	3.82	1.91	0.502	-3.20	2.68	3.20	6.00	61.06	66.95
S9	-5.31	-2.64	2.67	1.34	0.75	-3.98	5.93	3.98	2.08	60.58	66.94
S12	-5.67	-2.43	3.24	1.62	0.62	-4.05	5.06	4.05	6.04	72.87	67.50
S13	-5.21	-1.21	4.00	2.00	0.50	-3.21	2.58	3.21	6.09	53.10	70.88
E4	-5.68	-1.82	3.86	1.93	0.52	-3.75	3.64	3.75	6.15	29.09	73.14
E5	-5.60	-2.20	3.40	1.70	0.59	-3.90	4.47	3.90	8.94	66.46	72.32
E7	-5.13	-1.18	3.95	1.98	0.51	-3.16	2.52	3.16	3.23	35.10	75.08

Molecular Docking Result of the Bioactive Compounds

Bioactive compounds and the standard drug were used as ligands for the docking studies. bioassays. Nine conformers of each ligand-enzyme complex were analysed, the one with the lowest binding energy was identified to be the best binding mode of the docked compound to the target enzyme. Tables 3 to 5 display the binding energy, protein residues, and hydrogen interaction, while Figures 2 to 4 show the 2D and 3D diagrams of the interactions observed.

Test compounds were docked to the active site of the glutathione peroxidase receptor (3KIJ). The results showed that these

compounds inhibit the protein's active site, with binding energy between -5.2 to -7.9 Kcal/mol. They perfectly snug into the active site of the receptor by interacting with the amino acid residue at the binding site (CYS-79). The binding energy of the compounds is lower than that of the standards and this indicates that the compounds had better affinity to the receptor than the standards. Compound S9 had the lowest value of binding energy, hence best antioxidant activities, this agrees with the experimental result. The interactions involved are conventional hydrogen bond, Carbon hydrogen bond, pi-alkyl, and pi-pi-T-shaped, pi-anion and various Van der Waal's forces of attraction. It was also observed that all ligands formed conventional hydrogen bond with ASP-83 (Table 3) and Van der Waal's forces of attraction with CYS-79 (active site residue). These bindings are very vital for receptor-ligand interaction and for strengthening the interactions.

The compounds were also docked with COX-2 receptors (1OQ5). The results (Tables 4) indicate effective inhibition of the receptor's active site. The binding energy ranged from -6.7 to -8.4 Kcal/mol, with compound S9 exhibiting better anti-inflammatory inhibitory activities. The observed interactions were Conventional hydrogen bond, pi-pi-T-shaped, pi-sigma, pi-alkyl, carbon-hydrogen bond, unfavorable donor-donor, and Van der Waal' forces of attraction.

The antiglycation activities of the studied compounds were evaluated using Receptor for Advanced Glycation End product (RAGE) (4LP5) as the molecular targets. The 4LP5 receptor formed stable complexes with the test compounds, with the binding energy shown in Table 5. The binding energy ranged from -5.0 to -6.4 Kcal/mol, suggesting that rutin had the best antiglycation inhibitory activities. compounds S6 and S7 had the best inhibitory activities among the test compounds. The complexes showed van der waals forces of interaction and pi-alkyl bond. They all showed hydrogen bond except compound S1 and E4. Other types of interaction observed in some of the complexes are carbon hydrogen bond, pi-cation, pi-sigma, pi-anion, alkyl, and halogen bond. Only compound S13 and rutin formed vander waals forces of interaction with one of the amino acid residues (ALA-21) in the active site of the protein.

Table 3: Binding Energy, Residue and Interactions Between Ligands and 3KIJ Receptor

Ligands	ΔG kcal/mol	Hydrogen Interactions	Amino Acid Residue

S1	-7.4	Asp83 (3.82)	Arg84, Asp78, Ser77, Phe125, Tyr130, Cys79, Thr82, Gln80
S7	-7.8	Asp83 (3.86)	Arg84, Gln80, Ser77, Thr82, Tyr130, Phe125, Asp78, Cys79
S9	-7.9	Tyr130 (5.86), Asp83 (3.86)	Asp78, Ser77, Phe125, Thr82, Cys79, Gln80, Arg84
S12	-7.8	Asp83 (3.92)	Phe125, Cys79, Thr82, Gln80, Ser77, Arg84, Leu81, Asp78
S13	-6.8	Asp83 (4.54, 3.52)	Arg84, Asp78, Ser77, Phe125, Tyr130, Cys79, Thr82, Gln80
Gallic acid	-5.4	Asp83 (4.07, 4.17), Cys79 (3.40)	Thr82, Gln80, ASP-78, Ser77, Phe125
N-acetyl-L-Cystine	-5.2	Arg84 (3.1, 4.80), Gln80 (3.7, 5.06) Cys79 (5.08), Asp83 (3.56),	Leu81, Gln80, Thr82, Tyr120, Phe125, Ser77, Asn85

Table 4: Binding Energy, Residue and Interactions Between Ligands and 1OQ5 Receptor

Ligands	ΔG kcal/mol	Hydrogen Interactions	Amino Acid Residue
S1	-7.4	Glu69 (7.43)	Trp209, Val143, Thr199, Pro202, Asn67, Leu60, Gln92, Asn62, Ile91, Phe131, His94, Thr200, Leu198, Val121
S9	-8.4	Pro202 (7.43) Thr199 (4.32) Thr200 (6.14)	Val135, Pro210, His94, Leu198, Val207, Val121 Ser197, Trp209, His199, Val143, Gln92, His96, Asn62, Phe131, Leu204

S12	-8.2	Pro202 (5.23, 4.85), Thr200 (4.44), Thr199 (2.59)	Leu204, Val135, Pro201, Val121, His94, Leu198, Leu141, val207, Val143, Trp209, His96, Asn67, Gln92, Asn62
S13	-8.0	Gln92 (5.35, 5.14), Thr199, (3.74), His96 (5.52)	Glu69, Ile91, Val121, Phe131, His119, Val207, Trp209, Leu198, Val143, THR-199, LIG:O (xii) HIS-96, LIG:H (xiii) GLU-106, Trp200, Asn67, Asn62, Pro202, Ala65
Ibuprofen	-6.7	His96 (5.77)	Phe131, Gln92, Val121, Leu198, Val143, His94 Trp209, His119, His96, Thr119, Thr200,

Table 5: Binding Energy, Residue and Interactions Between Ligands and 4lp5

Ligands	ΔG kcal/mol	Hydrogen Interactions	Amino Acid Residue
S1	-5.4	Ala28 (3.72, 6.72)	Tyr113, Lys37, Val35, Leu34, Thr27, Arg216, Glu32, Arg29, Val89, Tyr118, Pro33, Ile26
S5	-5.8	Pro33 (4.98), Arg29 (6.03)	Tyr113, Lys37, Leu36, Leu34, Ala28, Val89, Glu32, Tyr 118, Thr27, Val35, Ile26, Gln24
S6	-6.2	Pro33 (4.49)	Tyr113, Leu36, Val35, Ala28, Leu34, Val89, Glu32, Arg29, Thr27, Ile26, Gln 24, Lys37
S7	-6.2	Glu32 (3.64), Tyr118 (5.41)	Tyr113, Lys37, Val35, Leu34, Pro33, Arg29, Thr27, Ala28, Leu37
S13	-5.4	Asn112 (5.20, 6.64)	Lys107, Gly40, lys39, Gln24, Ala23, Ser111, Gly20, Ala21, Met22, Lys110, Thr109.
E4	-5.1	Nil	Ile26 Thr27, Glu32, Arg29, Ala28, Leu34, Pro33, Val35, Gln24, Tyr113, Lys37
E5	-5.2	Thr27 (5.88), Pro33 (5.66)	Lys37, Ile26, Leu36, Val35, Leu34, Ala28, Arg29, Glu32, Tyr118, Arg216, Tyr113
E7	-5.0	Gln24 (5.51)	Lys39, Ala28, Glu32, Arg29, Thr27, Tyr118, Ile26, Val35, Leu36 Tyr113, Leu34, Lys37

Rutin	-6.4	Asn112 (3.79, 4.07), Ser111 (4.36), Lys110 (4.64, 4.43), Thr (3.9) Lys-39 (3.84, 3.60), Ala23 (3.95)	Met22, Gln24, Ala121, Gly20

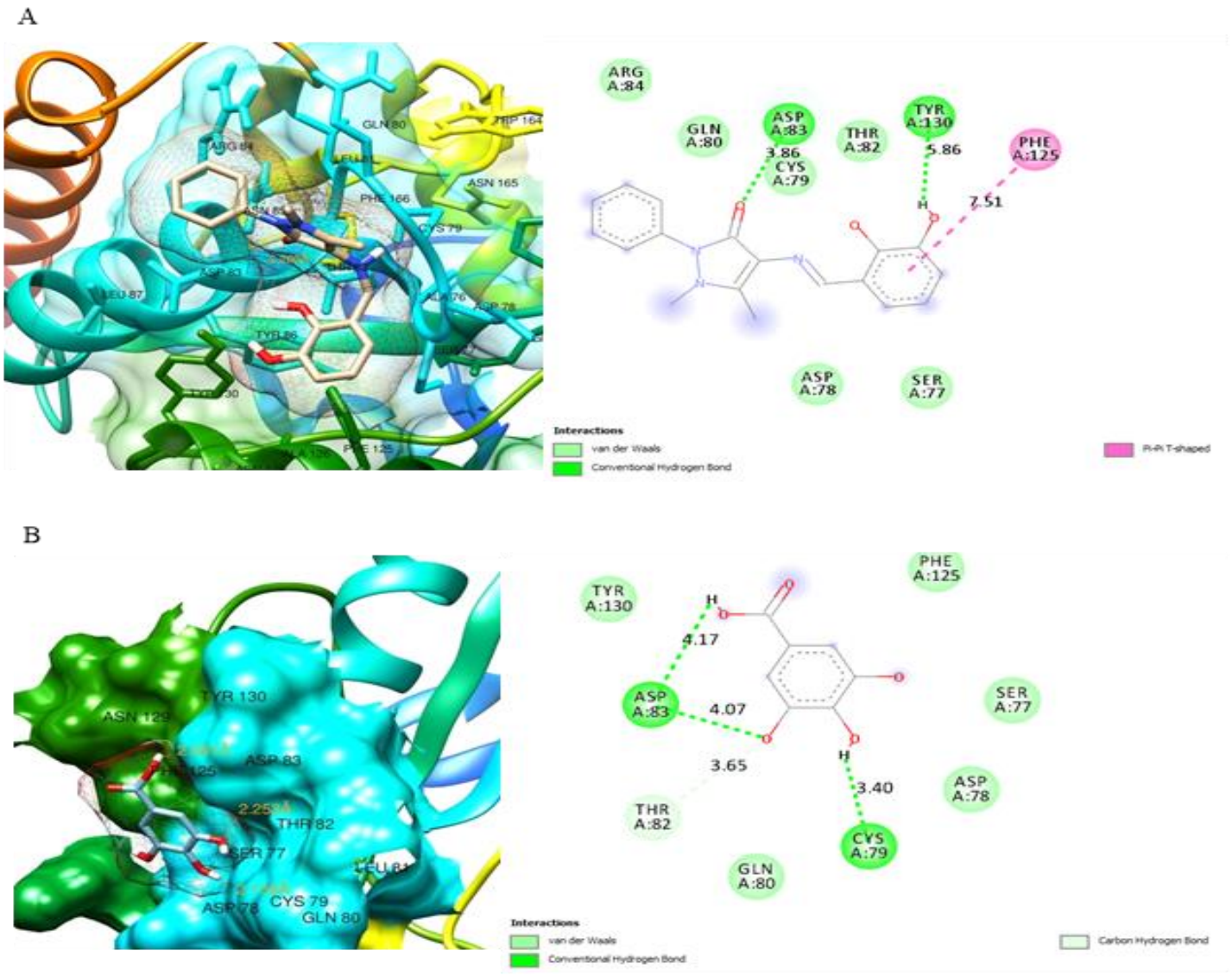

Figure 2: 3D (left) and 2D (right) Views of the Molecular Interactions of Amino Acid Residues of Glutathione Peroxidase (3KIJ) with (A) S9 (B) Gallic Acid.

A

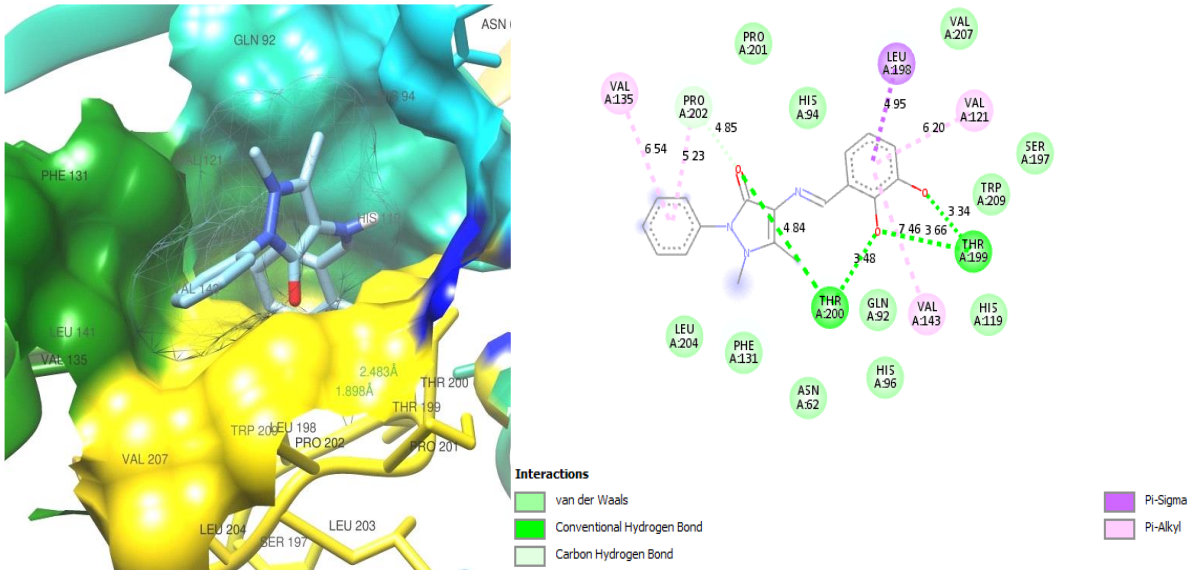

B

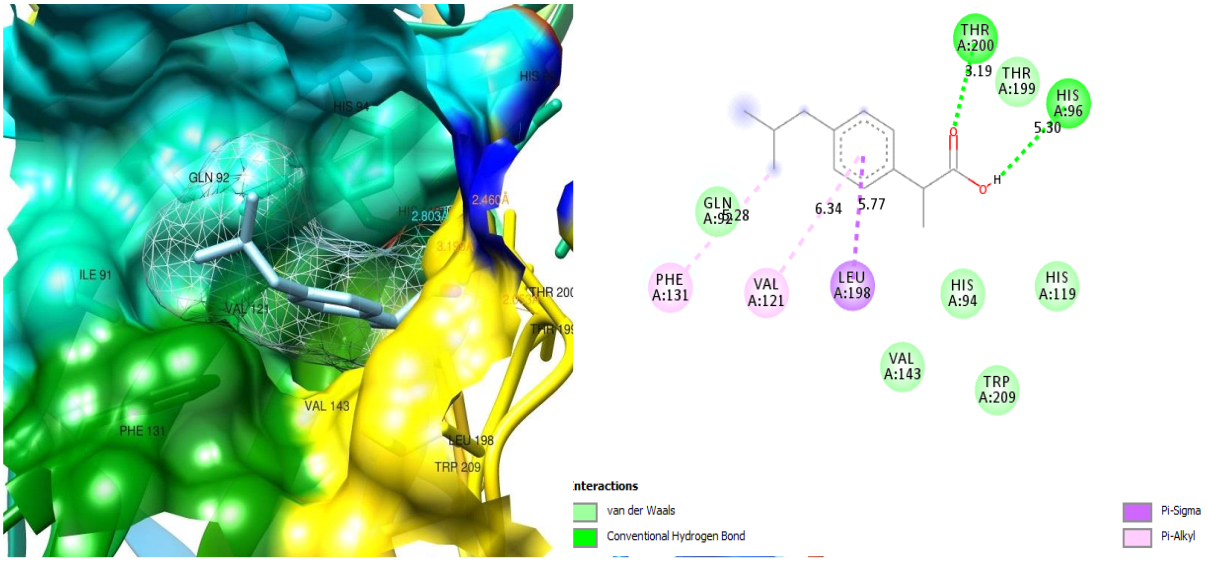

Figure 3: 3D (left) and 2D (right) Views of the Molecular Interactions of Amino-Acid Residues of COX-2 (1OQ5) with (A) S9, (B) Ibuprofen

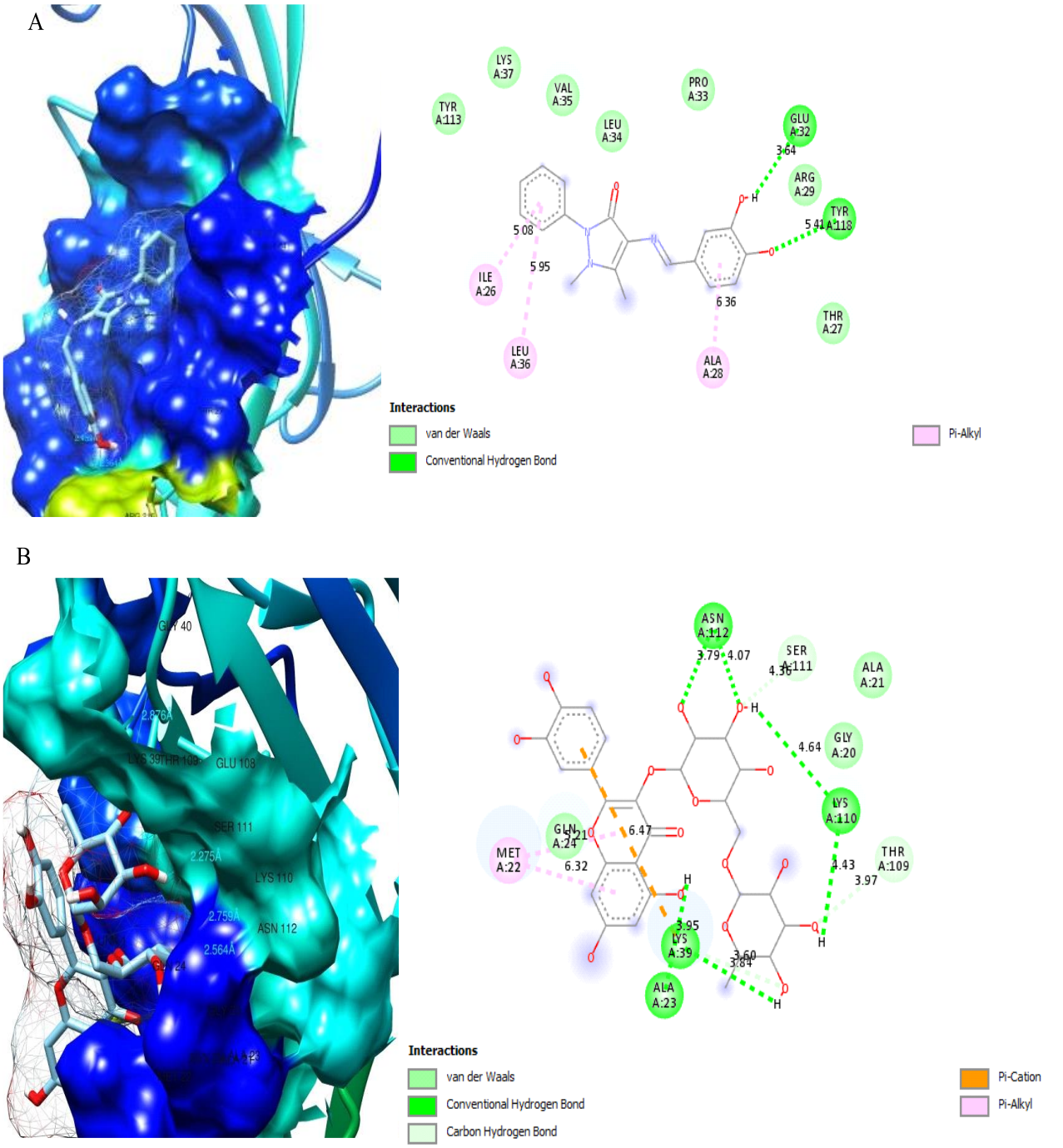

Figure 4: 3D (Left) and 2D (Right) Views of The Molecular Interactions of Amino-acid Residues of RAGE (4LP5) with (A) S7 (B) Rutin

4ADMET Profiling of the Bioactive Compounds

Some of the investigated substances showed potential in inhibiting target proteins. To assess how well they will operate pharmacologically as

medications, research on their ADMET properties is required. In silico ADMET prediction method can evaluate if these compounds are absorbable, distributable, metabolizable, and removable without side effects [53]. Tables 6 to 9 display the drug-likeness, lipophilicity, pharmacokinetics, and toxicity profiles of these compounds.

Drug-likeness is assessed through compound structure or properties. High TPSA and weight hinder penetration. All compounds, except E4, have three rings and two heteroatoms (N and O). E4 has four heteroatoms. Rutin has five rings, Gallic acid and ibuprofen have one ring and one heteroatom. N-acetyl-L-cysteine has no rings but two heteroatoms. All, except E4, adhere to Lipinski, Ghose, Veber, Egan, and Muegge rules ensuring risk-free oral absorption. E4 violates one Lipinski rule due to weight. Gallic acid and N-acetyl-L-cysteine violate Ghose and Muegge rules. Rutin violates several rules. The test compounds demonstrated very excellent drug-likeness properties when compared with the standards.

Lead-likeness of the test compounds, which defines physicochemical boundaries for a good lead, was analysed. The rule of three was applied: log P $\leq$ 3, MW < 300 daltons, $\leq$ 3 HBD, $\leq$ 3 HBA, and $\leq$ 3 rotatable bonds [54]. Compounds S1, S5, S7, S9, and S12 had no lead-likeness violations, while others and control drugs had one (Table 6). Compounds E4 and E7 had two, making them unfit further for evaluation. Hence other test compounds except E4 and E7 are fit for further optimization.

The Synthetic Accessibility (SA) score gauges a compound's ease of synthesis [55], with the analysed compounds scoring well (1.22-3.58), aside from rutin (6.52). Lipophilicity and water solubility are key properties affecting drug behaviour [56]. Drugs need a balance of lipophilicity for membrane penetration and hydrophilicity for blood circulation. Higher Log P values point to greater lipophilicity and reduced water solubility, influencing drug absorption [37]. Gallic acid, rutin, and N-acetyl-L-cysteine with very low Log P values -0.08, -1.29, and 0.21, respectively are observed to be very soluble (Table 7). The synthesized compounds and Ibuprofen had Log P values of 2.24 to 4.64 and were soluble to moderately soluble. This may be due to the presence of additional polar side chains in their structure.

Water solubility (Log S), predicted via the SILICOS-IT model, affects drug dissolution, with lower Log S values being preferable [57]. The compounds' Log S values (-0.81 to -5.89) trend is perfectly in accordance with the values of Log P earlier discussed. The bioavailability score, using total charge, TPSA, and the Lipinski filter, estimates the likelihood of compounds being good oral drugs [58]. With bioavailability scores of 0.55 for synthesized compounds, 0.86 for ibuprofen, 0.56 for gallic acid and N-acetyl-L-cysteine, and 0.17 for rutin (Table 7), these compounds show about a 55% chance of

minimum 10% oral absorption, suggesting they could be effective oral drugs [59].

Table 8 presents the pharmacokinetics prediction results of the test compounds. Skin permeability (Log Kp) evaluates molecules for transdermal administration [60]. More negative log Kp values mean less skin permeability [61]. Cytochrome P450 monooxygenase catalyzes many drug metabolism reactions, and non-inhibition against these enzymes suggests high bioavailability upon oral administration [62,63]. All synthesized compounds, except S9, potentially inhibit CYP2C9. E4, E5, and E7 potentially inhibit CYP2C19, while E5, E7, and Gallic acid potentially inhibit CYP3A4. None inhibits CYP2D6 and CYP1A2. Notably, S9, ibuprofen, and N-acetyl-L-cysteine do not inhibit any cytochrome P450. The plasma membrane ATP-binding transporter, P-glycoprotein (P-gp), effluxes xenobiotics to protect the body from foreign chemicals. All synthesized compounds and standard, except rutin, are permeability Pgp substrates. They have a high potential for gastrointestinal tract absorption, suggesting possible oral administration absorption [64]. The liver, being defenseless against toxic agents and various drugs, can be damaged by human hepatotoxicity (H-HT), potentially leading to organ failure [24]. The mutagenicity test identifies potentially mutagenic compounds [65]. The toxicity prediction of these compounds is favorable (Table 4.26).

ProTox II toxicity prediction classifies all synthesized compounds, except S5 (10000 mg/kg) and E5 (7500 mg/kg), as oral toxicity class 6 with LD50 5600 mg/kg. Only compounds S6 and E5 showed potential mutagenicity due to the presence of a nitro substituent. Thus, all synthesized compounds are relatively safe as therapeutic agents. Gallic acid, N-acetyl-L-cysteine, ibuprofen, and rutin fall under different oral toxicity classes with varying LD50 and mutagenicity probabilities [66].

The synthesized compounds showed acceptable outcomes in drug-likeness, lipophilicity, pharmacokinetics, and toxicity prediction compared to standard drugs.

Table 6: Drug-likeness Prediction Output of Test Compounds

Code	MW	HBD	HBA	MR	TPSA	SA	Lipinski violation	Ghose violation	Veber violation	Egan violation	Muegge violation	Lead-likeness
S1	337	1	4	98.47	68.75	3.14	0	0	0	0	0	0
S5	309	1	3	91.98	59.52	2.99	0	0	0	0	0	0
S6	352	1	5	100.80	105.34	3.22	0	0	0	0	0	1
S7	323	2	4	94.00	79.75	3.06	0	0	0	0	0	0
S9	323	2	4	94.00	79.75	3.12	0	0	0	0	0	0
S12	339	3	5	96.02	99.98	3.19	0	0	0	0	0	0
S13	357	5	1	104.96	77.98	3.32	0	0	0	0	0	1
E4	458	0	3	116.93	48.52	3.39	1	0	0	0	0	2
E5	390	0	5	113.04	94.34	3.46	0	0	0	0	0	1
E7	399	0	4	118.49	57.75	3.58	0	0	0	0	0	2
GAL	170	4	5	39.47	97.99	1.22	0	1	0	0	1	1
CYSTEINE	163	2	3	38.85	105.20	2.08	0	3	0	0	1	1
IBF	206	1	2	62.18	37.30	1.92	0	0	0	0	0	1
RUTIN	610	10	16	141.38	269.43	6.52	3	4	1	1	4	1

Code	iLOGP	XLOGP3	WLOGP	MLOGP	Silicos-IT Log P	Consensus Log P	ESOL Log S	Solubility Class	BS
S1	3.34	3.11	2.95	2.22	3.03	2.93	-4.13	M. soluble	0.55
S5	2.87	1.77	2.94	2.53	2.98	2.62	-3.21	soluble	0.55
S6	2.58	2.97	3.37	1.54	1.21	2.33	-4.12	M. soluble	0.55
S7	2.56	2.79	2.65	1.99	2.49	2.50	-3.93	Soluble	0.55
S9	2.65	1.41	2.65	1.99	2.49	2.24	-3.06	Soluble	0.55
S12	3.04	2.43	2.35	1.46	2.01	2.26	-3.78	Soluble	0.55
S13	3.53	1.71	2.96	1.91	3.09	2.64	-3.33	Soluble	0.55
E4	3.92	4.9	4.74	4.22	5.44	4.64	-5.89	M.soluble	0.55
E5	3.38	3.41	3.76	2.16	2.36	3.01	-4.45	M.soluble	0.55
E7	4.41	3.67	3.42	3.17	4.82	3.90	-4.59	M.soluble	0.55
GAL	2.17	0.7	0.5	0.2	-0.2	0.21	-1.64	V soluble	0.56
CYSTEINE	0.65	0.36	-0.49	-0.54	-0.36	-0.08	-0.81	V.soluble	0.56
IBF	2.17	3.5	3.07	3.13	3.15	3.00	-3.36	Soluble	0.86
RUTIN	1.58	-0.33	-1.69	-3.89	-2.11	-1.29	-3.3	V.soluble	0.17

Table 7: Predicted Lipophilicity (Log P) Values, Water Solubility and Bioavailability

GAL: Gallic acid; Cysteine: N-acetyl-L-cysteine; IBF: Ibuprofen; MW: Molecular weight; HBD: Hydrogen bond donor, HBA; Hydrogen bond Acceptor, TPSA: Topological Polar Surface Area; SA: Synthetic Accessibility

Table 8: Pharmacokinetics Prediction Output of Test Compounds

Code	GI	P.gp	CYP 1A2	CYP2 C19	CYP 2C9	CYP2 D6	CYP 3A4	Log KP (cm/s)
S1	High	No	No	No	Yes	No	No	-6.15
S5	High	No	No	No	Yes	No	No	-6.92
S6	High	No	No	No	Yes	No	No	-6.34
S7	High	No	No	No	Yes	No	No	-6.29
S9	High	No	No	No	No	No	No	-7.27
S12	High	No	No	No	Yes	No	No	-6.64
S13	High	No	No	No	Yes	No	No	-7.33
E4	High	No	No	Yes	Yes	No	No	-5.62
E5	High	No	No	Yes	Yes	No	Yes	-6.26
E7	High	No	No	Yes	Yes	No	Yes	-6.13
GAL	High	No	No	No	No	No	Yes	-6.84
CYSTEINE	High	No	No	No	No	No	No	-7.04
IBF	High	No	No	No	No	No	No	-5.07
RUTIN	Low	Yes	No	No	No	No	No	-10.26

GI: gastrointestinal; P-gp: P-glycoprotein.

Table 9. Toxicity Profiles of Test Compounds

Code	LD50 (mg/kg)	Toxicity Class	Hepato-toxicity	Carcinoge-nicity	Immune-toxicity	Mutage-nicity	Cytoto-xicity
S1	5600	6	-	-	-	-	-
S5	10000	6	-	-	-	-	-

S6	5600	6	-	-	-	+	-
S7	5600	6	-	-	-	-	-
S9	5600	6	-	-	-	-	-
S12	5600	6	-	-	-	-	-
S13	5600	6	-	-	-	-	-
E4	5600	6	-	-	-	-	-
E5	7500	6	-	-	-	+	-
E7	5600	6	-	-	-	-	-
GAL	2000	4	-	-	-	-	-
CYSTEINE	4400	5	-	-	-	+	-
IBF	299	3	+	-	-	-	-
RUTIN	5000	5	-	-	+	-	-

Conclusion

The results revealed that all the synthesized compounds were not toxic, and some possessed antioxidant, anti-inflammatory, and antiglycation activities. These compounds could serve as leads in the formulation of drugs for the management of inflammation, oxidative stress, and aging. The position and nature of the substituent attached to the compound can greatly affect its biological activities. It was observed that compounds that possessed -OCH3 and OH groups exhibited greater biological activity The study showed that compounds with antioxidant and inflammatory potential could serve as antiglycation agents as demonstrated by compounds S1 and S13. Therefore, antioxidant and anti-inflammatory compounds possessing OH and OCH_3 substituents should be explored more in the future for the investigation of antioxidant, anti-inflammatory, and antiglycation activities. Also, further optimization and in vivo testing should be considered.

Author Contributions

The authors collectively contributed to the creation of the manuscript and have approved the final version of the manuscript. Credit: **EAE** conceptualization, data curation, investigation, methodology, fund acquisition, writing-original draft. **BBA**-conceptualization, validation, formal analysis, supervision, writing-review and editing.

Acknowledgments

We acknowledge The World Academy of Science for the Award of the 2018 ICCBS-TWAS Sandwich Postgraduate Fellowship awarded to Ms. Erazua Ehimen Annastasia (FR number: 3240305617). We also acknowledge Dr. Hina Siddiqui, and Prof. M. Iqbal Choudhary, at the International Center for Chemical and Biological Sciences University of Karachi, Pakistan where the fellowship was tenable.

Conflicts of Interest

The authors declare no conflict of interest.

References

[1] Deshmukh, P., Soni, K. P., Kankoriya, A., Halve, K. A. and Dixit. R. (2015). 4-Aminoantipyrine: A Significant Tool for the Synthesis of Biologically Active Schiff Bases and Metal Complexes. *International Journal of Pharmaceutical Science Review Research,* 34(1): 162-170.

[2] Suhta, A., Saral, S., Çoruh, U., Karakuş, S. and Vazquez-Lopez, E.M. (2024). Synthesis, Single Crystal X-Ray, Hirshfeld Surface Analysis and DFT Calculation Based NBO, HOMO–LUMO, MEP, ECT and Molecular Docking Analysis of N′-[(2, 6-Dichlorophenyl) Methylidene]-2-{[3-(Trifluoromethyl) Phenyl] Amino} Benzohydrazide. *Journal of Structural Chemistry,* 65(1): 196-215.

[3] Elemike, E. E., Onwudiwe, D. C., Nwankwo, H. U. and Hosten, E. C. (2017). Synthesis, crystal structure, electrochemical and anti-corrosion studies of Schiff base derived from o-toluidine ando-chlorobenzaldehyde. *Journal of Molecular Strucure,* 1136: 253-262.

[4] Kashyap, S., Kumar, S., Ramasamy, K., Lim., S. M., Ali Shah, S. A., Om, H. and Narasimhan, B. (2018). Synthesis, biological evaluation, and corrosion inhibition studies of transition metal complexes of Schiff base. *Chemistry Central Journal,* 12:117.

[5] Murtaza, S., Akhtar, M. S., Kanwal, F., Abbas, A., Ashiq, S. and Shamam, S. (2017). Synthesis and biological evaluation of Schiff base of 4-aminophenazone as anti- inflammatory, analgesic, and antipyretic agents. *Journal of Saudi Chemical Society,* 21: S359-S372.

[6] Aguilar-Llanos, E., Carrera-Pacheco, S.E., González-Pastor, R., Zúñiga-Miranda, J., Rodríguez-Pólit, C., Mayorga-Ramos, A., Carrillo-Naranjo, O., Guamán, L.P., Romero-Benavides, J.C., Cevallos-Morillo, C. and Echeverría, G.A. (2023). Crystal Structure, Hirshfeld Surface Analysis, and Biological Activities of Schiff-Base Derivatives of 4-Aminoantipyrine. *American Chemical Society omega,* 8 (45): 42632-42646.

[7] Chavan, R. R. and Hosamani, K. M. (2018). Microwave-assisted synthesis, computational studies and antibacterial/anti-inflammatory activities of compounds based on coumarin-pyrazole hybrid. *Royal Society open science,* 5:172435.

[8] Shaikh, S., Dhavan, P., Singh, P., Uparkar, J., Vaidya, S.P., Jadhav, B.L. and

Ramana, M.M.V. (2023). Design, synthesis and biological evaluation of novel antipyrine based α-aminophosphonates as anti-Alzheimer and anti-inflammatory agent. *Journal of Biomolecular Structure and Dynamics*, 41 (2): 386-401.

[9] Asiri, A. M. and Khan, S. A. (2010). Synthesis and Anti-Bacterial Activities of Some Novel Schiff Bases Derived from Aminophenazone. *Molecules,* 15: 6850-6858.

[10] Shoaib, M., Rahman, G., Ali, S. W. and Naveed, M. U. (2015). Synthesis of 4-aminoantipyrine derived Schiff bases and their evaluation for antibacterial, cytotoxic, and free radical scavenging activity. *Bangladesh Journal of Pharmacology*, 10: 332-336.

[11] Aguilar-Llanos, E., Carrera-Pacheco, S. E., González-Pastor, R., Zuniga-Miranda, J., Rodriguez-Polit, C., Romero-Benavides, J. C. and Heredia-Moya, J. (2022). Synthesis and Evaluation of Biological Activities of Schiff Base Derivatives of 4-Aminoantipyrine and Cinnamaldehydes. *Chemistry Proceedings*, 12(1): 43-57.

[12] Cakmak, R., Basaran, E., Boga, M., Erdogan, O., Ercan, C. and Cevik. O. (2022). Schiff Base Derivatives of 4-Aminoantipyrine as Promising Molecules: Synthesis, Structural Characterization, and Biological Activities. *Russian Journal of Bioorganic Chemistry,* 48: 334-344.

[13] Kasare, M. S., Dhavan, P. P., Shaikh, A. H., Jadhav, B. L. and Pawar, D. L, (2022). Novel Schiff base scaffolds derived from 4-aminoantipyrine and 2-hydroxy-3-methoxy-5-(phenyldiazenyl) benzaldehyde: Synthesis, antibacterial, antioxidant and anti-inflammatory. *Journal of Molecular Recognition*, 35(9): 2976-2985.

[14] Kang, Q. and Yang, C. (2020). Oxidative stress, and diabetic retinopathy. Molecular mechanisms, pathogenetic role and therapeutic implications. *Redox Biology* 37: 2213-2317.

[15] Kumar, M., Padmini, T. and Ponnuve, T. (2017). Synthesis, characterization, and antioxidant activities of Schiff bases are of cholesterol. *Journal of Saudi Chemical Society*, 21: S322-S328.

[16] Martemucci, G., Portincasa, P., Ciaula, A. D., Mariano, M., Centonze, V. and Alessandro, A. G. (2022). Oxidative stress, aging, antioxidant supplementation and their impact on human health: An overview. *Mechanisms of Ageing and Development*, 206: 111-127.

[17] Nowotny, K., Jung, T., Hohn, A., Weber, D. and Grune, T. (2015). Advanced glycation end products and oxidative stress in type 2 diabetes mellitus. *Biomolecules* 5(1): 194- 222.

[18] Oguntibeju, O. O. (2019). Type 2 diabetes mellitus, oxidative stress, and inflammation: examining the links. *International Journal of Physiology*, 1511(3): 45-63.

[19] Erazua, E. A., Oyebamiji, A. K. and Adeleke, B. B. (2018) DFT-QSAR and Molecular Docking Studies on 1,2,3-Triazole-Dithiocarbamate Hybrids as Potential Anticancer Agents. *Physical Science International Journal*, 20.4: 1-10.

[20] Erazua, E. A. and Adeleke, B. B. (2019) DFT and Molecular Docking Investigation of Potential Anticancer Properties of Some Flavonoids. *Journal of Pure and Applied Chemistry Research*, 8.3: 225-231.

[21] Guan, L., Yang, H., Cai, Y., Sun, L., Di, P., Li, W., Liu, J. and Tang, Y. (2019). ADMET-score a comprehensive scoring function for evaluation of chemical drug-likeness. *Medicinal Chemistry Communication*, 10: 148-157.

[22] Wu, F., Zhou, Y., Li, L., Shen, X., Chen, G., Wang, X., Liang, X., Tan, M. and Huang, Z. (2020). Computational Approaches in Preclinical Studies on Drug Discovery and Development. *Frontiers in Chemistry*, 8.2: 1-32.

[23] Erazua, E. A., Oyebamiji, A. K., Akintelu, S. A., Adewole, A. D., Adelakun, A. and Adeleke, B. B. (2023). Quantitative Structure-Activity relationship, Molecular Docking and ADMET Screening of Tetrahydroquinoline Derivatives as Anti-Small Cell Lung Cancer Agents. *Eclética Química*, 48.1: 55-71.

[24] Babalola, B. A, Adetobi, T. E, Akinsuyi, O. S, Adebisi, O. and Folajimi, E. O. (2021). Computational Study of the Therapeutic Potential of Novel Heterocyclic Derivatives against SARS-CoV-2. *Covid 1*, 4: 757-774.

[25] Borase, J. N., Mahale, R. G. and Rajput, S. S. (2021). Synthesis and Biological Evaluation of Heterocyclic Schiff Bases: A Review. *International Journal of Pharmaceutical Research*, 13(2): 188-202.

[26] Singh, G., Satija, P., Singh, B., Sinha, S., Sehgal, R. and Sahoo, S. C. (2020). Design, crystal structures and sustainable synthesis of family of antipyrine derivatives: Abolish to bacterial and parasitic infection. *Journal of Molecular Structure*, 1199: 127-139.

[27] Banti, C. N. and Hadjikakou, S. K. (2021). Evaluation of Toxicity with Brine Shrimp Assay. *Bio-protocol*, 11(2): 3895-3910.

[28] Suryawanshi, V. S., Yadav, A. R., Mohite, S, K. and Magdum, C. S. (2020). Toxicological Assessment using Brine Shrimp Lethality Assay and Antimicrobial activity of Capparis Grandis. *Journal of University of Shanghai for Science and Technology*, 22 (11): 746-759.

[29] Karatas, M. O., Tekin, S., Alici, B. and Sandal, S. (2019). Cytotoxic effects of coumarin substituted benzimidazolium salts against human prostate and ovarian cancer cells. *The Journal of Chemical Sciences*, 131(69): 1647-1659.

[30] Leah, Q., Scott, K. R., Finn, S. P., Hayes, M. and Gray, S. G. (2020). An In Vitro Study Determining the anti-inflammatory activities of sinapinic acid-containing extracts generated from Irish rapeseed meal. *Medical Research Archives*, 8(10): 2375-2394.

[31] Sethi, S., Joshi, A., Arora, B., Bhowmik, A., Sharma, R. R. and Kumar, P. (2020). Significance of FRAP, DPPH, and CUPRAC assays for antioxidant activity determination in apple fruit extracts. *European Food Research and Technology*, 246: 591-598.

[32] Starowicz, M. and Zielinski, H. (2019). Inhibition of Advanced Glycation End-Product Formation by High Antioxidant-Leveled Spices Commonly Used in European Cuisine. *Antioxidants*, 8(4):100-113.

[33] Becke, A. D. 1993. Density-functional thermochemistry. III. The role of exact exchange. *Journal of Chemical Physics*, 98: 5648-5652.

[34] Yang, L., Feng, J. and Ren, A. (2005). Theoretical studies on the electronic and optical properties of two thiophene-fluorene based π-conjugated copolymers. *Polymer*, 46:10970-10982.

[35] Geerlings, P., De Proft, F., and Langenaeker, W. (2003). Conceptual density functional theory. *Chemical reviews*, 103:1793-1873.

[36] Parr, R. G., Szentpaly, L. V. and Liu, S. (1999). Electrophilicity Index. *Journal of the American Chemical Society*, 121 (9): 1922-1924.

[37] Johnson, T. O., Adegboyega, A. E., Iwaloye, O., Eseola, O. A, Plass, W., Afolabi, B., Rotimi, D., Ahmed, E., Albrakati, A., Batiha, G. E. and Adeyemi, O. S. (2021) Computational study of the therapeutic potentials of a new series of imidazole derivatives against SARS-CoV-2. *Journal of Pharmacological Sciences*, 147 (1), 62-671https://doi.org/10.1016/j.jphs.2021.05.004

[38] Savino, D.F., Silva, J.V., da Silva Santos, S., Lourenço, F.R. and Giarolla, J. (2024). How do physicochemical properties contribute to inhibitory activity of promising peptides against Zika Virus NS3 protease? *Journal of Molecular Modeling*, 30 (2): 54.

[39] Tang, S., Ding, J., Zhu, X., Wang, Z., Zhao, H. and Wu, J. (2023). Vina-GPU 2.1: towards further optimizing docking speed and precision of AutoDock Vina and its derivatives. *bioRxiv*, 11: 455-461.

[40] Valdés-Tresanco, M. S., Valdés-Tresanco, M. E., Valiente, P. A. and Moreno, E. (2020) AMDock: a versatile graphical tool for assisting molecular docking with Autodock Vina and Autodock4. *Biology direct*, 15(1):1-12.

[41] Xia, Y., Pan, X., and Shen, H. B. (2024). A comprehensive survey on protein-ligand binding site prediction. *Current Opinion in Structural Biology*, 86: 102793.

[42] Daina, A., Michielin, O.and Zoete, V. (2017). SwissADME: a free web tool to evaluate pharmacokinetics, druglikeness and medicinal chemistry friendliness of small molecules. *Scientific Report*, 7(1): 42717 DOI: 10.1038/srep42717.

[43] Banerjee, P., Eckert, A. O., Schrey, A. K. and Preissner, R. (2018) ProTox-II: a web server for the prediction of toxicity of chemicals. *Nucleic Acids Research*, *46* (W1), W257-W263. https://doi.org/10.1093/nar/gky318

[44] Lipinski, C. A., Lombardo, F., Dominy, B. W. and Feeney, P. J. (2001). Experimental and computational approaches to estimate solubility and permeability in drug discovery and development settings. *Advance Drug Delivery Review*, 46 (1): 3-26.

[45] Veber, D. F., Johnson, S. R., Cheng, H. Y., Smith, B. R., Ward, K. W. and Kopple, K. D. (2002). Molecular properties that influence the oral bioavailability of drug candidates. *Journal of medicinal chemistry,* 45.12: 2615-2623.

[46] Tok, F., Kocyigit-Kaymakcıoglua, B., Saglıkb, N., Levent, S., Ozkay, Y. and Kaplancıklı, Z. A. (2019). Synthesis and biological evaluation of new pyrazolone Schiff bases as monoamine oxidase and cholinesterase inhibitors. *Bioorganic Chemistry,* 84: 41-50.

[47] Teran, R., Guevara, R., Mora, J., Dobronski, L., Barreiro-Costa, O., Beske, T. Pérez-Barrera, J., Araya Maturana, R., Rojas-Silva, P., Poveda, A. and Heredia-Moya, J. (2019). Characterization of Antimicrobial, Antioxidant, and Leishmanicidal Activities of Schiff Base Derivatives of 4-Aminoantipyrine. *Molecules,* 24: 2696-2978.

[48] Zaater, S., Bouchoucha, A., Djebbar, S. and Brahimi, M. (2016). Structure, vibrational analysis, electronic properties, and chemical reactivity of two benzoxazole derivatives: functional density theory study. *Journal of Molecular Structure,* 1123: 344-354.

[49] Erazua, E. A., Akintelu, S. A., Adelowo, J. M., Odoemene, S. N., Josiah, O. M., Raheem, S. M., Latona, D. F., Adeoye, M. D., Esan, A. O. and Oyebamiji, A. K. (2021). QSAR and Molecular Docking Studies on Nitro (Triazole/Imidazole)-Based Compounds as Anti-Tubercular Agents. *Tropical Journal of Natural Product Research,* 5(11): 2022-2029.

[50] Adebesin, T. T., Oladosu, I. A., Obi-Egbedi, N. O and Odika, T. I. (2016). Demetallation, antimicrobial and computational studies of methoxy-1,3-diene substituted products from addition of natural products to tricarbonyl-2-methoxycylohexadienyl) iron tetra fluoborate. *Journal of organometallic Chemistry,* 819: 87-94.

[51] Erazua, E. A. and Adeleke, B. B. (2019). A Computational Study of Quinoline Derivatives as Corrosion Inhibitors for Mild Steel in Acidic Medium. *Journal of Applied Science and Environmental Management,* 23.10: 1819-1824.

[52] Costa, J. S., Ramos, R. S., Costa, K. L. S., Brasil, D. S. B., Silva, C. H. T., Ferreira, E. F. B., Borges, R. S., Campos, J. M., Macedo, W. J., and Santos, C. B. R. (2018). An In Silico Study of the Antioxidant Ability for Two Caffeine Analogs Using Molecular Docking and Quantum Chemical Methods. *Molecules,* 23: 2801-2818.

[53] Guan, L., Yang, H., Cai, Y., Sun, L., Di, P., Li, W., Liu, J. and Tang, Y. (2019). ADMET-score is a comprehensive scoring function for evaluation of chemical drug-likeness. *Medicinal Chemistry Communication,* 10: 148-157.

[54] Bon, M., Bilsland, A., Bower, J. and McAulay, K. (2022). Fragment-based drug discovery-the importance of high-quality molecule libraries. *Molecular Oncology,* 16(21): 3761-3777.

[55] Swierczewska, M., Lee, K. C. and Lee, S. (2015). What is the future of PEGylated therapies. *Expert Opinion on Emerging Drugs,* 20 (4): 531-539.

[56] Zarmpi, P., Flanagan, T., Meehan, E., Mann, J. and Fotaki, N. (2020). Impact of Magnesium Stearate Presence and Variability on Drug Apparent Solubility Based on Drug Physicochemical Properties. *American Association of Pharmaceutical Scientists,* 22(4): 75-93.

[57] Ditzinger, F., Price, D. J., Ilie, A., Kohl, N. J., Jankovic, S., Tsakiridou, G., Aleandri, S., Kalantzi, L., Holm, R., Nair, A., Saal, C., Griffin, B. and Kuentz, M. (2019). Lipophilicity and hydrophobicity considerations in bio-enabling oral formulations approaches. *Journal of Pharmacy and Pharmacology,* 71(4): 464-482.

[58] Ferreira, L. G. and Andricopulo, A. D. (2019). ADMET modeling approaches in drug discovery. *Drug Discovery Today,* 24(5):1157-1165.

[59] Xu, Y., Li, Y., Xie, J., Xie, L., Mo, J. and Chen. W. (2021). Bioavailability, Absorption, and Metabolism of Pelargonidin-Based Anthocyanins Using Sprague-Dawley Rats and Caco-2 Cell Monolayers. *Journal of Agricultural and Food Chemistry,* 69(28): 7841-7850.

[60] Iyer, A., Jyothi, V. G., Agrawal, A., Khatri, D. K., Srivastava, S., Singh, S. B. and Madan, J. (2021). Does skin permeation kinetics influence efficacy of topical dermal drug delivery system: Assessment, prediction, utilization, and integration of chitosan biomacromolecule for augmenting topical dermal drug delivery in skin. *Journal of Advanced Pharmaceutical Technology and Research,* 12(4): 345-355.

[61] Coderch, L., Collini, I., Carrer, V., Barba, C. and Alonso, C. (2021). Assessment of Finite and Infinite Dose In Vitro Experiments in Transdermal Drug Delivery. *Pharmaceutics,*13(3): 364.

[62] Sen, A. and Stark, H. (2019). Role of cytochrome P450 polymorphisms and functions in development of ulcerative colitis. *World Journal of Gastroenterology,* 25(23): 2846-2862.

[63] Esteves, F., Rueff, J. and Kranendonk, M. (2021). The Central Role of Cytochrome P450 in Xenobiotic Metabolism-A Brief Review on a Fascinating Enzyme Family. *Journal of Xenobiotics,* 11(3): 94-114.

[64] Rathod, S., Desai, H., Patil, R. and Sarolia, J. (2022). Non-ionic Surfactants as a P-Glycoprotein(P-gp) Efflux Inhibitor for Optimal Drug Delivery-A Concise Outlook. *Journal of the American Association of Pharmaceutical Scientists,* 23(1): 55-69.

[65] Goyal, K., Goel, H., Baranwal, P., Dixit, A., Khan, F., Jha, N. K., Kesari, K. K., Pandey, P., Pandey., Benjamin, M., Maurya, A., Yadav, V., Sinh, R. S., Tanwar, P., Upadhyay, T. K., and Mittan, S. (2022). Unravelling the molecular mechanism of mutagenic factors impacting human health. *Environmental Science and Pollution Research,* 29: 1993-62013.

[66] Noga, M., Michalska, A. and Jurowski, K. (2024). The acute toxicity of Novichok's degradation products using quantitative and qualitative toxicology in silico methods. *Archives of Toxicology*,